Coherent states in a Rydberg atom: Classical mechanics

Ernestine Lee,[1] Andrea F. Brunello,[1,2] and David Farrelly[1]
[1]*Department of Chemistry and Biochemistry, Utah State University, Logan, Utah 84322-0300*
[2]*Department of Physics, State University of New York, Stony Brook, New York 11794-3800*
(Received 26 August 1996)

The interaction of a hydrogen or Rydberg atom with a circularly polarized microwave field leads to the creation of global equilibrium points that may be stable or unstable depending on the particulars of the applied field. The additional application of a magnetic field, perpendicular to the plane of polarization, can be used to manipulate both the nature and the stability of these points. We show that stable three-dimensional motion can be maintained that is localized at either a maximum or a minimum in the corresponding surface of zero velocity. At these equilibria, the zero-velocity surface may be locally quadratic in coordinates and stable harmonic-oscillator-like, nondispersive, coherent states can be supported. As the fields are varied, repeated order-chaos transitions may be observed, including various passages through rigorously integrable limits. Classical simulations are presented for a range of field strengths, and the effects of deviations of the microwave field from exactly circular polarization (i.e., elliptical polarization) are examined using a pulsating zero-velocity surface. [S1050-2947(97)07103-5]

PACS number(s): 32.80.Rm, 05.45.+b, 42.50.Hz, 92.10.Cg

I. INTRODUCTION

The development of wave mechanics forced the abandonment of the idea that a physical path could be ascribed to an atomic electron, thereby demolishing the concept of a classical or planetary atom [1–3]. Nevertheless, a modern interpretation of what constitutes a ''classical atom'' [4] can still be suggested as follows: (i) the wave packet that represents the electron is localized in space, neither spreading nor dispersing as its center moves along a Kepler orbit; (ii) the guiding classical orbit is confined to a single plane in space (interestingly, the configuration so produced would correspond physically to a rotating giant dipole [5]). Recent studies of ''the classical limit of an atom'' that follow this definition have emphasized the creation of nondispersive electronic wave packets in Rydberg atoms whose motion will follow a Kepler orbit [6,7]. In actuality, there have been a number of attempts to construct quasiclassical or coherent states for the Kepler problem, going back to the pioneering work of Schrödinger. These attempts have met with varying degrees of success, although, ultimately, the states that have been suggested have all eventually been found to spread [8–18]. Recently, however, Klauder has proposed a positive resolution of this long-standing problem, showing that the construction of coherent states for the bound part of the hydrogen atom is possible [19].

In order to assemble a wave packet without dispersion, a quantum system with constant or almost constant energy-level spacings is necessary [20–22]. For the harmonic oscillator itself the construction of nonspreading, nondispersive states is obviously straightforward—the energy level spacings are constant and truly nondispersive coherent states are possible. Indeed, the original concept of coherent states was developed by Schrödinger for the harmonic oscillator [11,23–25]. In contrast to the isotropic harmonic oscillator, the energy-level spacings of the hydrogen atom are clearly not constant. Yet, the identity between the hydrogen atom and a four-dimensional (4D) isotropic oscillator with constraints (obtained, e.g., via the Kustaanheimo-Stiefel transformation [26,27]) has been exploited by Barut and Xu [28] to show theoretically that nonspreading, almost Gaussian states for the Kepler problem are possible, at least theoretically. These wave packets ''ride'' along Kepler orbits and are constrained to the plane of the orbit. The complicated functional form of these states raises delicate issues of preparation, especially in the adjustment of the phase of the initial wave packet, which turns out to be critical to the long-term stability of the Xu-Barut states.

The strategy that has proved most successful *in practice* in the preparation of nonspreading electronic wave packets and for investigating the semiclassical and classical limits of an atom is to work at very high quantum numbers, usually in the presence of external fields, to create regimes in which the local energy spacings are approximately constant [4,6,29–33,17,34–38]. Laser excitation is used to form a spatially well-localized superposition of these states, which may mimic a coherent state for a sufficiently large number of Kepler periods as to permit their manipulation in experiments (e.g., analogs of Young's double-slit interferometry experiment, except using matter waves [39]). For example, adiabatic switching for atomic beams in crossed electric and magnetic fields has been used to form circular states [40–44]. The atomic beam undergoes multiphoton excitation in a region where the electric field dominates to populate the ''linear'' state, which is then adiabatically turned into a circular state with the beam passing into a region where the magnetic field dominates. The spatial orientations of the angular momentum **L** and the Runge-Lenz vector **A** are controlled by the external fields, and coherent elliptic states may be formed [45] that qualify as minimum uncertainty states [46,47]. Nevertheless, these packets eventually disperse; the best that has been accomplished experimentally has been the creation of atoms in which the spreading of the wave packet is concentrated along the Kepler orbit—i.e., long-term radial

but not angular confinement [4,6].

In this paper we adopt a different strategy in that we use external fields to continuously stabilize the packet as it moves around the nucleus; in essence, the states are coherent states of an atom dressed by particular external fields. Specifically, a combination of circularly polarized (CP) microwave and magnetic fields is used to create new global equilibrium points in a rotating frame and, associated with these equilibria, there may be nondispersive coherent states if (a) the equilibrium is *stable* and (b) the regime surrounding the equilibrium point is locally harmonic in a region that is large compared to the wavelength of the electron (one aim of this paper is to estimate the sizes of such harmonic regions). The resulting states, therefore, are (in this approximation) actually identical to conventional coherent states since the local Hamiltonian is a harmonic oscillator. To be sure, these states are not those sought by Schrödinger; despite this, the present approach represents a way of ''parking'' an electron in an orbit far from the core or nucleus in a fashion similar to the motion of a satellite around the Earth.

In fact, considerable interest has resurfaced recently in the creation of field-maintained coherent atomic states, and this work stems, in part, from the independent discovery by Farrelly and Uzer [48] and Bialynicki-Birula *et al.* [49] of stable equilibria for a hydrogen atom in a circularly polarized microwave field [50–57,48,58]. These equilibria are analogous to gravitational equilibrium points in the restricted three-body problem of celestial mechanics [59,60]. Bialynicki-Birula *et al.* [49] recognized that wave packets launched from these points will be expected to orbit the nucleus without spreading, provided the field parameters are chosen such that the equilibrium point, which is a *maximum*, is stable. Clearly, stable maxima are not common in atomic systems, and much is to be learned by comparison with perhaps the most well-known example of stable motion at a maximum, the dynamics of Jupiter's Trojan asteroids, whose existence was expected from Lagrange's studies of the three-body problem going back to 1772 [59]. Like their celestial counterparts (L_4 and L_5) whose stability can be attributed to the interplay of Coriolis and gravitational forces, the atomic Lagrangian equilibrium points are stable over only a quite limited range of parameters. Associated with the atomic maximum is a transition to instability—essentially an atomic Trojan bifurcation—as the electric-field strength is increased [48,61]. Beyond this bifurcation the quantum wave packet, which has become known as a Trojan state, will certainly be expected to spread. An additional complication, however, is that, if the linear regime surrounding the equilibrium point is smaller than the effective wavelength of the electronic wave packet the wave packet will spread by leakage from the stable region. We have argued recently that atoms of unrealistically large diameter would need to be prepared to guarantee that the electronic wavelength could fit into the locally linear region surrounding the equilibrium [62,63]. Incidentally, contrary to misstatements in [64], in Ref. [62] we argue that the size of the stability region surrounding the Trojan equilibrium point is insufficient, for a reasonably sized atom, to support a *Gaussian* wave packet rather than being too small to support any quantum states. We now summarize several different approaches to minimizing spreading of the Trojan wave packets.

Bialynicki-Birula and co-workers [63,65] themselves recognized the possibility of increasing the stability properties of their original Gaussian wave packet [49] by modifying its shape; actually, the curved Trojan they arrived at semiempirically can be thought of as resulting from an attempt to approximate the true eigenstates supported by the equilibrium point. The spectrum of the time-independent Hamiltonian in the rotating frame (in the vicinity of the equilibrium) supports a ladder of eigenstates, each of which is spatially localized in the proximity of the Lagrange point. A Gaussian wave packet (with appropriately chosen frequencies) is really a zeroth-order approximation to the lowest such state. The curved wave packet used in Refs. [63, 65, 66] (also relevant for stabilization in linearly polarized microwave fields [67]) is simply a better approximation to this state, and, indeed, this packet was found to have better stability properties than the original packet used by Bialynicki-Birula *et al.* [49]. In the opposite limit one would obviously choose an exact eigenstate as the initial wave packet, since such an eigenstate of the (rotating-frame) Hamiltonian can never disperse. An extension of the approach used by Bialynicki-Birula and co-workers [63,65] to refine their initial packet is to perform a full diagonalization of the Hamiltonian and identify states that are localized at the equilibrium point. This will produce numerically accurate Trojan wave packets and is the approach that Zakrzewski and co-workers [68,69] have recently adapted to obtain Trojan eigenstates. Zakrzewski and co-workers [68,69] actually computed resonance wave functions using the complex-coordinate method in a Floquet calculation [70]. An alternative is a conventional complex-coordinate calculation in the rotating frame [71]. In any case, all of these approaches amount to recognizing the existence of eigenstates of the Hamiltonian (in the rotating frame) that have enhanced probability density remote from the nucleus and concentrated close to the equilibrium point. It should be emphasized that such states are not coherent states; in principle, any eigenstate of any Hamiltonian in a rotating frame qualifies as a nondispersive, nonstationary eigenstate, but the Trojans are unusually interesting because most of their probability density is localized away from the core. However, the preparation of exact eigenstates of this system may be difficult to actually implement in an experiment. Further, small displacements of the eigenstates from the equilibrium point will tend to cause the packets to spread; the beauty of a coherent state is that such a state is robust to displacements within the harmonic region surrounding the equilibrium point.

For these reasons, an alternative strategy is in order in which the emphasis is on preparing good approximations to harmonic-oscillator coherent states by manipulating the stability properties of the Lagrange equilibrium points themselves. The groundwork may be laid by the addition of a magnetic field perpendicular to the plane of polarization of the CP field [48]. In this paper, we extend our earlier analysis of the maximum [72], and, using classical mechanics, show that a magnetic (B) field in combination with a CP microwave field can be used to stabilize genuinely 3D coherent states in this system. For certain combinations of fields we also show that the problem may actually become integrable.

Motion at a maximum, whether stable or unstable, is precarious both classically and quantum mechanically. In celes-

tial mechanics, dissipation, e.g., will cause particles (asteroids) localized at the Lagrange points to fall down the energy maximum and ultimately to be lost. In the atomic problem, while dissipation is not an issue, because the maximum is not surrounded by potential walls a wave packet can tunnel into nearby chaotic regions of phase space and thus, eventually ionize, perhaps by chaos-assisted tunneling. Evidence for this is found in the classical simulations we present that show that the stable equilibrium is surrounded by a huge chaotic sea. Quantum calculations of Zakrzewski *et al.* [69] reveal that the widths of the Trojan resonances fluctuate considerably with field parameters, similar to conductance fluctuations in mesoscopic systems, underscoring the delicate balancing act an electron at the maximum must undergo to remain stable.

The problems associated with dynamics at a *maximum* can be alleviated with the discovery that it is possible to form a stable outer *minimum* in the effective potential using a slightly different field configuration [73,74]. The minimum configuration has a couple of advantages: (a) a particular, experimentally accessible, limit is rigorously integrable; and (b) even in cases where the dynamics within the well is chaotic, the electron can still be strongly localized away from the core—the only way it can approach the core is by tunneling through what may be a very substantial barrier. In Ref. [74] it was shown that a ladder of nondispersive, nonstationary eigenstates is associated with this minimum and many of the eigenstates were calculated explicitly. Depending on the field parameters the classical mechanics may be chaotic and eigenstates scarred by unstable periodic orbits were found. In many ways the system mimics an electron trap such as the Penning trap: a number of recent articles have, in fact, developed analogies between atomic Rydberg electrons and the dynamics of charged particles in the Paul and Penning traps [75–78] as well as the motion of a neutral atom in a so-called wire trap [79]. Similar phenomena exist in both, and it is, therefore, valuable to compare the detailed dynamics of both types of system. One example is the chaotic heating or diffusion in momentum space that is found both in the microwave ionization of Rydberg atoms and in rf heating of ions in a Paul trap [80,81]. A second is the problem of a hydrogen atom in a generalized van der Waals potential, which has recently been shown to share identical integrable limits with the Paul trap (in the pseudopotential approximation) [82,83].

Some time ago Clark, Korevaar, and Littman [84] suggested the possibility of a single Rydberg atom functioning as a quasi-Penning (QP) trap: the system proposed was a hydrogen atom subjected to crossed electric and magnetic fields for which long-living resonances associated with the Stark saddle point were predicted [84]. However, the spectral signature expected from the QP orbits has not, so far, been detected [85,86]. In this paper we show that, by a judicious choice of the sense of the polarization of the CP field, its frequency, and the magnetic-field strength, it is possible to localize the electron in a harmonic potential well in a region of space that excludes the nucleus—essentially a double well is produced in the effective potential. This is in a rotating frame. In the laboratory frame the electronic wave packet is localized both radially and in an angular sense—the packet travels along circular orbits lying beyond the Stark saddle point, even for extremely high electric-field strengths. The problem thus satisfies the general criterion for a classical atom: localization of a wave packet both in an angular and a radial sense in a 2D Keplerian orbit. In a frame rotating with the CP field frequency, the system resembles an atom in crossed electric and magnetic fields and may, therefore, be considered to constitute a microscopic QP or Rydberg atom trap [73].

In the context of a Rydberg atom in crossed electric and magnetic fields—denoted throughout as the $E\times B$ system [86–91]—a number of workers have postulated the existence of an ''outer'' well in the atomic potential [92–95]. In this field configuration the linear Zeeman or paramagnetic term (proportional to the component of electronic angular momentum along the magnetic-field direction) is not conserved and can, therefore, be thought of as a velocity-dependent perturbation that mixes coordinates and momenta. The difficulty in treating such a term has led to a number of analyses that essentially ignore the paramagnetic term because its presence prevents the separation of the Hamiltonian into kinetic and potential parts. In the absence of the paramagnetic contribution, under certain conditions, the potential in the $E\times B$ system may display an outer well [92–95]. Despite the uncontrolled approximations involved, these studies have engendered experimental research directed to observing the unusually large atomic dipoles that might be expected to result from such a well [5]. Unfortunately, simply ignoring the paramagnetic term is a rather poor approximation and, in actuality, the ''potential-energy'' function that results may or may not possess an outer well, depending on the gauge used; in other words, the approximation results in an unphysical, i.e., gauge-dependent potential [5,92–95]. More recently, Cederbaum and co-workers [96] have demonstrated that an outer minimum can be created in the atomic $E\times B$ problem if the finite mass of the nucleus is taken into account, but the remoteness from the nucleus of the resulting, relatively shallow, well makes it unclear how easy it would be to observe the consequences of this well in an experiment.

The approach we develop is gauge invariant and uses the concept of a zero-velocity surface (ZVS) to handle the paramagnetic term. In the $E\times B$ system it is easy to demonstrate that an outer well cannot exist in the effective potential (in the infinite nuclear mass approximation), but, for the combined magnetic and CP fields we study, as already noted, global equilibria corresponding to maxima or minima can be readily produced and visualized using the ZVS. In the rotating frame, therefore, all of the suggestions put forward as to the possible consequences of an outer potential well in the $E\times B$ system (giant dipoles, etc.) apply to this system, with the significant additional merits that such a well is not only (a) expected to exist theoretically, but (b) is also expected to be experimentally realizable.

This paper studies the classical mechanics of the hydrogen atom simultaneously subject to a CP microwave and an orthogonal magnetic field and reports extensive simulations that suggest that stable coherent wave packets can be supported quantum mechanically. The companion paper [97] describes quantum simulations of the time-dependent Schrödinger equation using fast-Fourier-transform (FFT) methods to propagate the wave packet. The paper is organized as follows: in Sec. II the Hamiltonian for the hydrogen atom in

combined CP and (perpendicular) magnetic fields is introduced, together with the concept of a zero-velocity surface, which is a method, adapted from celestial mechanics, to visualize the dynamics in problems that feature velocity-dependent (Coriolis) forces. Here we show how the direction of the magnetic field and the choice of polarization of the CP field can be used to produce either a maximum or a minimum in the effective potential. In each case, a second equilibrium point, a saddle point, is shown to exist. A stability analysis of the equilibrium points in this problem is presented in Sec. III, where it is shown that the B field can not only stabilize the equilibrium points but can also extend the volume of phase space that is locally harmonic around the equilibrium point. Further, an integrable limit of this problem is identified. Section IV is given over to a series of 3D classical simulations; in particular, we propagate swarms of trajectories with initial conditions chosen to simulate coherent atomic states. In this section we also investigate the transition from regular to chaotic motion as the field parameters are varied. Of course, in an actual experiment it may be difficult to produce and maintain a CP field for which the polarization is exactly circular. Thus we have also performed a series of simulations to study the possible effects of ellipticity of the microwave field on the stability of the motions. Conclusions are in Sec. V.

II. CLASSICAL HAMILTONIAN AND EQUILIBRIUM POINTS

The Lagrangian for a hydrogen atom (in atomic units $a_0=\hbar=e=\mu=1$ and assuming an infinite nuclear mass) subjected simultaneously to a CP microwave field (field strength F and frequency ω_f) and a static magnetic field perpendicular to the plane of polarization of the CP field is

$$\mathcal{L}=\frac{\dot{x}^2+\dot{y}^2+\dot{z}^2}{2}+\frac{1}{r}-\frac{\pm\omega_c}{2}(x\dot{y}-y\dot{x}) \pm F(x\cos\omega_f t+y\sin\omega_f t), \tag{1}$$

where ω_c is the cyclotron frequency (sometimes denoted as the reduced magnetic-field strength, $B/B_0=B/2.35\times10^5$ T in atomic units), and the choice of sign in the paramagnetic term is determined by the direction of the magnetic field. The sign of F is immaterial but our convention is to choose this sign such that any global equilibria corresponding to maxima or minima will turn out to lie along the positive x axis. At this point we note that, by virtue of Cauchy's uniqueness theorem, a particle starting out in the plane of polarization, with an initial velocity contained in that plane, will never leave the plane [98]. This is useful in that the reduced problem is amenable to the computation of surfaces of section. The time dependence in Eq. (1) may be eliminated by going to a frame that rotates at the constant angular velocity ω_f, which finally leads to the Hamiltonian

$$H=K=\frac{p_x^2+p_y^2+p_z^2}{2}-\frac{1}{r}-\omega(xp_y-yp_x) \mp Fx+\frac{\omega_c^2}{8}(x^2+y^2), \tag{2}$$

where K is analogous to the Jacobi constant in the restricted three-body problem (RTBP) and $\omega=(\omega_f\mp\omega_c/2)$. The presence of a nonconserved velocity-dependent (paramagnetic) term in the Hamiltonian prevents the separation of H into a positive-definite quadratic form in momenta and a potential-energy term. Nevertheless, a type of potential—in the language of celestial mechanics, a zero-velocity surface—can be constructed and provides an excellent starting point for studying the dynamics [59,60]. The first step is to rewrite the Hamiltonian, using Hamilton's equations of motion, in terms of *velocities* rather than momenta, which gives

$$H=\frac{\dot{x}^2+\dot{y}^2+\dot{z}^2}{2}-\frac{1}{r}\mp Fx-\frac{\omega_f(\omega_f\mp\omega_c)}{2}(x^2+y^2). \tag{3}$$

Note that the kinetic part is now positive definite in momenta and the ZVS is defined

$$V=H-\frac{\dot{x}^2+\dot{y}^2+\dot{z}^2}{2}=-\frac{1}{r}\mp Fx-\frac{\omega_f(\omega_f\mp\omega_c)}{2}(x^2+y^2). \tag{4}$$

While level curves of the ZVS may be used to provide information on the location and nature of equilibrium points and the locations of classically allowed and forbidden regions, unlike a *potential*-energy surface, such level curves need provide no information on the linear stability of equilibrium points, unless those equilibria are saddles. More directly, a maximum in a ZVS might be stable or unstable, and some analysis must be performed to determine stability. A key point of the Hamiltonian (2) is that this configuration of fields allows the coefficient of the paramagnetic term to be varied or even eliminated. Equilibria of the ZVS are obtained by requiring that all first partial derivatives of the ZVS vanish, i.e., $\partial V/\partial q_i=0$ with $q_i=(x,y,z)$. The equilibrium points are found to occur in pairs: depending on the sign chosen in Eq. (1) either a saddle and a maximum or a saddle and a minimum are produced. These cases will be referred to as the maximum and minimum configurations.

A. The maximum configuration

Taking the + sign in Eq. (4) with $\omega_c\geq0$ results in the zero-velocity surface

$$V=-\frac{1}{r}+Fx-\frac{\omega_f(\omega_f+\omega_c)}{2}(x^2+y^2), \tag{5}$$

with the equilibrium points lying on the x axis as given by the solutions of the equations

$$F+1/x_0^2-\omega_f(\omega_c+\omega_f)x_0=0 \tag{6}$$

for the maximum and

$$F-1/x_0^2-\omega_f(\omega_c+\omega_f)x_0=0 \tag{7}$$

for the saddle point. For conciseness x_0 is used to refer simply to any equilibrium point. When it is necessary to specifically differentiate between the saddle and the maximum and the minimum, the obvious notations $x_0^{\max(\min)}$ and x_0^{sad} will be used. Figure 1 is an isometric plot of the 2D ZVS, with $\omega_c=0$ showing the locations of L_s and $L_m^{\max}$. It is the latter

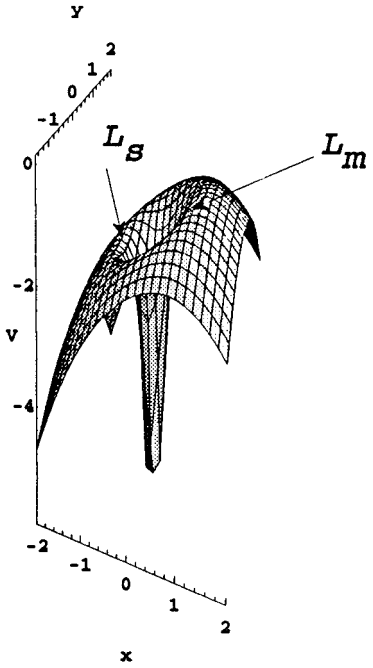

FIG. 1. Isometric view of the ZVS in scaled units as defined in Eq. (24) with $F=0.6$, $\omega_c=0$, $\omega_f=1$. The saddle L_s and the maximum L_m are shown.

that provides the analogy with the Lagrange equilibrium points L_4 and L_5 in the RTBP. Note that this configuration of equilibria is preserved even on the addition of a magnetic field ($\omega_c \neq 0$), provided that the Larmor frequency and the helicity of the wave are chosen such that the plus sign emerges in Eq. (2). However, the *stability* of these points, and the size of the regime supporting linear dynamics around the maximum will be affected by the relative magnitudes of F, ω_f, and ω_c, as will become apparent.

We pause to remark that the analysis of Ref. [49] is based on the launching of wave packets centered on $L_m^{\max}$ in the pure CP limit. These packets will be good approximations to the ideal nondispersive coherent state only if the size of the locally harmonic regime surrounding $L_m^{\max}$ is large compared to the wavelength of the electron. In the classical limit, a trajectory started precisely at $L_m^{\max}$ will remain at that point, but dressing such a periodic orbit (a circular orbit in the laboratory frame) with a Gaussian wave packet opens up the possibility of spreading due to nonlinearities and chaos. Of course, the nature of both classical and quantal motion at a stable maximum differs considerably from the more usual case of motion at a minimum; e.g., deviations from perfect circular polarization might tend to destabilize the maximum by producing time-dependent driving terms, i.e., the absence of confining potential walls means that the wave packet can escape the vicinity of the maximum by leakage into nonlinear regimes. Bialynicki-Birula and co-workers [63,65] have pointed out that quantum effects may act to confine the wave packet, even though the classical dynamics will tend to escape. This is due to the existence of a so-called ''quantum potential,'' which, e.g., in 1D for the Schrödinger equation $H\phi(x)=E\phi(x)$ is given by $V_Q(x)=-(\hbar^2/2m)\phi''(x)/\phi(x)$. However, this term will be repulsive for a perfectly Gaussian wave function. Inclusion of higher-order terms in the expansion at the maximum (essentially preparing a differently shaped wave packet) might lead to enhanced stability. On the other hand, it might not.

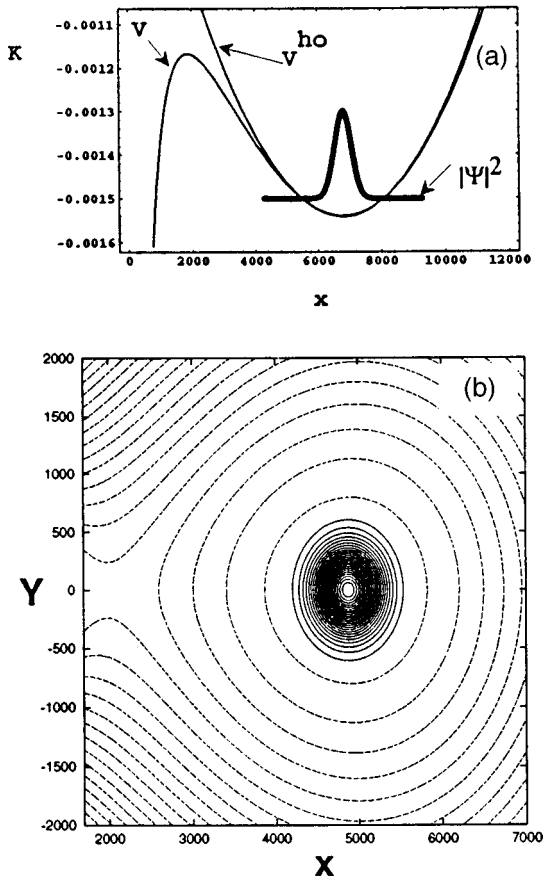

FIG. 2. (a) Zero-velocity surface for the minimum configuration with $\omega_c=3.46$ T, $\omega_f=50$ GHz, and $F=2000$ V/cm. A section ($y=z=0$) through the potential is shown. Also plotted is the harmonic approximation to the potential V^{ho}, and the Gaussian probability density of the ground state $|\Psi|^2$. (b) Level curves of the ZVS together with contours of the ground state as obtained by Taylor expansion about the minimum. The parameters are the same as in (a).

B. The minimum configuration

Selection of the $-$ sign in Eq. (4), with $\omega_c>0$, results in an entirely different critical point topology. Again the equilibria occur along the x axis as solutions of equations

$$F-1/x_0^2-\omega_f(\omega_c-\omega_f)x_0=0 \tag{8}$$

for the minimum and

$$F+1/x_0^2-\omega_f(\omega_c-\omega_f)x_0=0 \tag{9}$$

for the saddle. We examined the nature and the stability of the critical points of the ZVS in this limit and found that a transition occurs at $F_c=3[\omega_f(\omega_c-\omega_f)]^{2/3}/\sqrt[3]{4}$. For $F<F_c$ the ZVS possesses no real critical points. At $F=F_c$ a real, double critical point is spawned that, with increasing F, splits into a saddle point and a minimum. Figure 2(a) is a section through the ZVS showing these features, together

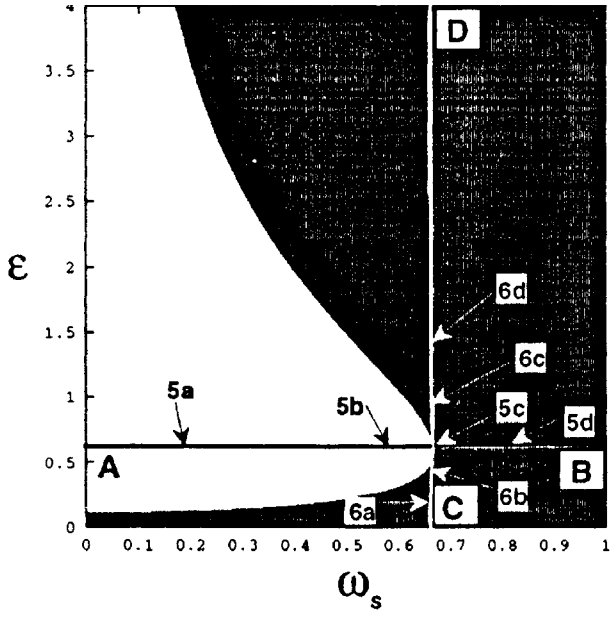

FIG. 3. Stability regions for the maximum configuration as a function of the scaled parameters ω_s and ϵ: stable (shaded) and unstable (unshaded). The lines AB and CD are described in the text and the labels $5a$, etc., refer to the surfaces of section in Figs. 5 and 6.

with a harmonic approximation to the minimum and an estimate of the ground-state wave function in the potential well. Figure 2(b) shows level curves of the ZVS and a contour plot of the ground-state wave function—details of how this wave function are calculated are supplied later. The depth of the well and its proximity to the nucleus depend sensitively on the field strengths. Note that for this field configuration ionization is impossible except along the z direction. Having established the existence of equilibria that are analogs of Lagrangian points in the RTBP, the next step is to understand the factors affecting the stability of the maximum and the spatial extent of any stable regions in comparison to the size of $\hbar$.

III. STABILITY ANALYSIS AND COHERENT STATES

The basic idea is to expand the Hamiltonian in a Taylor series at a global equilibrium point; if the expansion is locally harmonic, then a coherent state (defined by the local frequencies) will be able to be prepared provided that the equilibrium point is linearly stable. Such a coherent state (in the rotating frame) will neither spread nor disperse as it executes motion along a Kepler orbit (the Kepler frequency of the electron is in a 1:1 resonance with the microwave frequency), although it might decay by tunneling. An additional and, in general, more significant source of dispersion will arise if the tails of the wave packet penetrate appreciably into nonlinear or chaotic parts of phase space. This is expected to

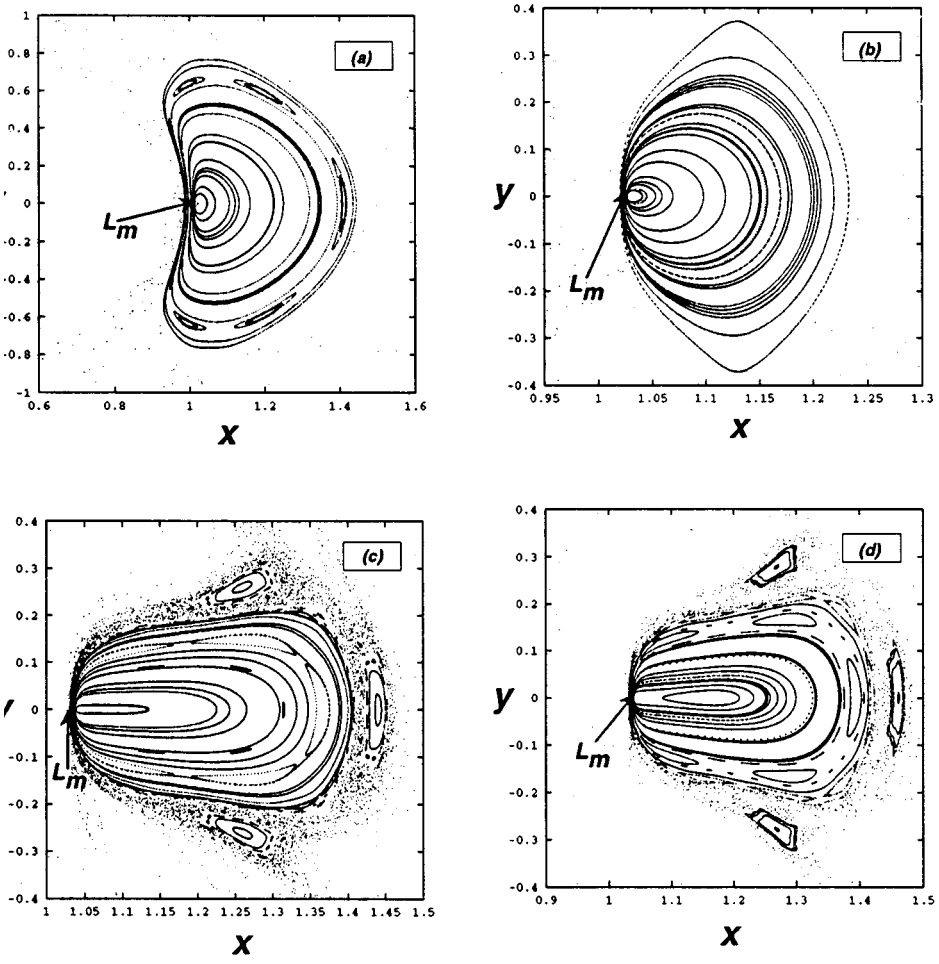

FIG. 4. Poincaré surfaces of section ($P_\rho = 0$) in scaled units showing the Trojan bifurcation with $\omega_c = 0$. In each case the energy is the energy of the maximum: (a) $\epsilon = 0.0444$, (b) $\epsilon = 0.1$, (c) $\epsilon = 0.1156$ (the Trojan bifurcation), (d) $\epsilon = 0.1170$.

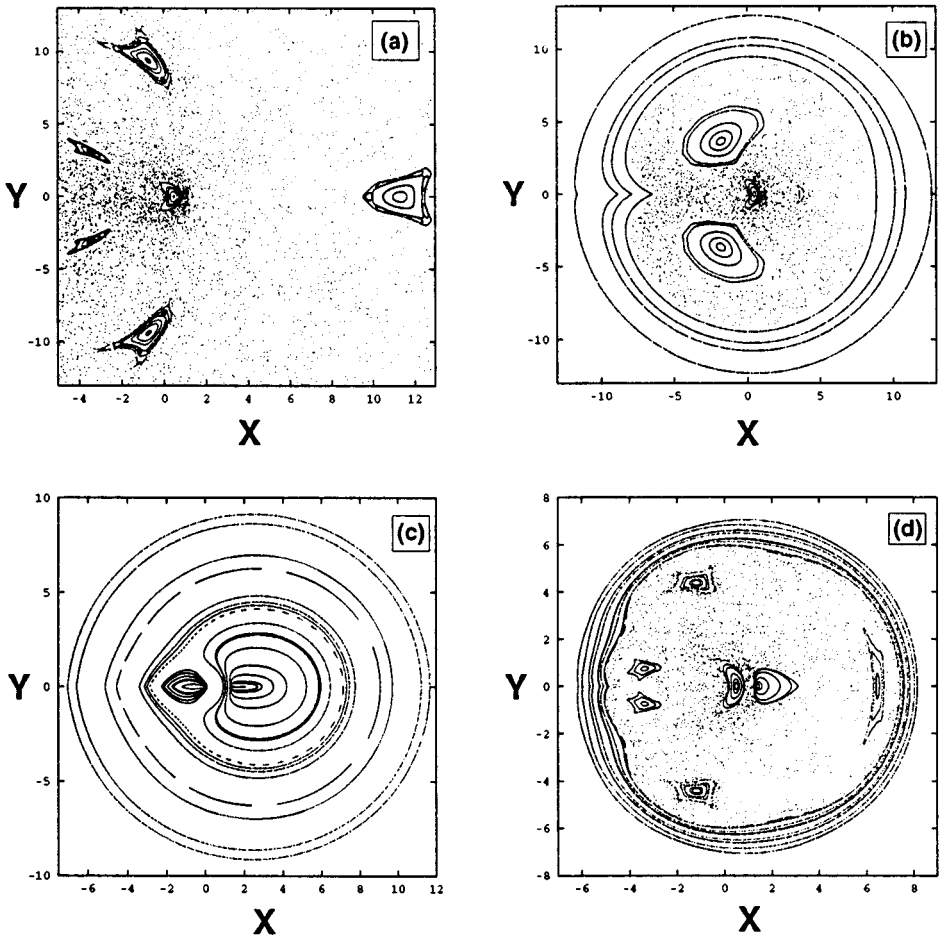

FIG. 5. Poincaré surfaces of section along the line AB in Fig. 3. In each case $\epsilon=0.6$ while ω_s is changed. (a) $\omega_s=0.2$, (b) $\omega_s=0.6$, (c) $\omega_s=\frac{2}{3}$, and (d) $\omega_s=0.8$.

be a bigger problem at the maximum than at the minimum. In the laboratory frame, if these dispersive factors can be minimized, the electronic wave packet will travel along a circular Kepler orbit while remaining localized radially and angularly for a finite (hopefully large) number of Kepler periods. An important point in our study is that the stability of such a packet can be enhanced considerably by using a magnetic field in tandem with the CP field.

Usually, stable motion at an equilibrium point in a Hamiltonian system can occur only at a potential-energy minimum. In many experimentally important problems the Hamiltonian can be separated into a sum of a positive-definite kinetic term depending quadratically on momenta and a potential part depending exclusively on coordinates, which prevents stable motion from occurring *other* than at a minimum [99]. While this is the most common situation in atomic physics, the problem in hand does not meet this criterion because of the presence of the *nonconserved* paramagnetic term, i.e., one cannot identify separate kinetic and potential parts of the Hamiltonian. Therefore, the stability of any equilibrium points must, in principle, be calculated explicitly; e.g., by computing the eigenvalues of the infinitesimally symplectic mapping governing the flow. Additionally, the paramagnetic term complicates the computation of the frequencies associated with the coherent state, since this bilinear perturbation must first be diagonalized.

In this section we show how to compute the appropriate frequencies at either a maximum or a minimum in the presence of the paramagnetic term. The procedure is essentially to prediagonalize a locally linear approximation to the Hamiltonian at the relevant equilibrium point. A stability analysis is only necessary for the maximum ($L_m^{\max}$) configuration because motion at a minimum that is to lowest order quadratic (as it is in the present case at $L_m^{\min}$), be it in a potential-energy or a zero-velocity surface, must always be linearly stable in a small enough domain around that equilibrium point. (A good account of the existence of stable maxima in celestial mechanics is provided by Greenberg and Davis [100].) For both the maximum and the minimum configurations the strategy about to be described is used to compute the functional form (specifically, the frequencies) of the initial coherent state. The steps involved are (a) a transformation to a synodic barycentric system of Cartesian coordinates at the equilibrium L_m, (b) expansion of the ZVS in a power series to second order—this produces what is known in nuclear physics as a cranked oscillator, (c) determination of the linear stability regime of the equilibrium point (for the maximum), and (d) computation of the vacuum state of the cranked oscillator.

A. Transformation to synodical barycentric coordinates at L_m and development of the cranked oscillator

The transformation from the original rotating (synodic) center of mass coordinates to the equilibrium configuration L_m is accomplished through the canonical transformation [101,102]

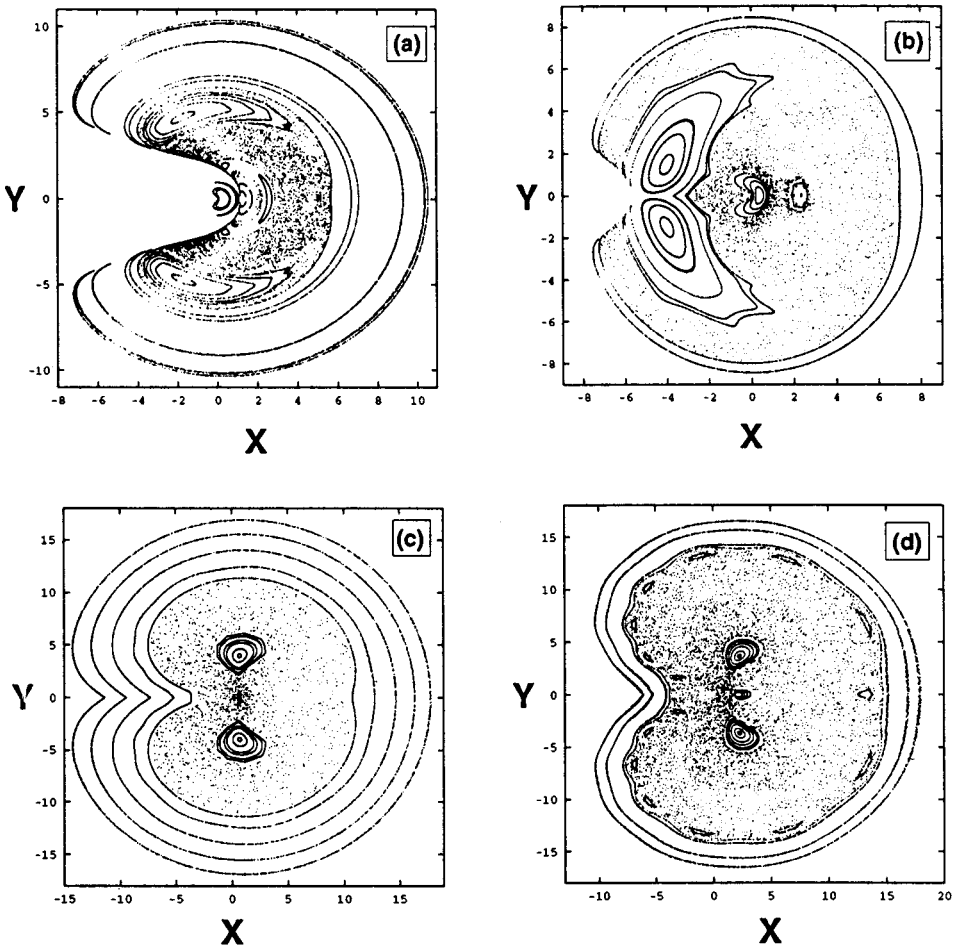

FIG. 6. Poincaré surfaces of section along the line *CD* in Fig. 3. In each case $\omega_s=\frac{2}{3}$, while ϵ is changed. (a) $\epsilon=0.2$, (b) $\epsilon=0.4$, (c) $\epsilon=1.0$, and (d) $\epsilon=1.5$.

$$x=x_0+\xi, \quad p_x=p_\xi,$$
$$y=\eta, \quad p_y=p_\eta+\omega x_0, \tag{10}$$
$$z=\zeta, \quad p_z=p_\zeta,$$

which transforms the Hamiltonian (2) into the form

$$H=\frac{p_\xi^2+p_\eta^2+p_\zeta^2}{2}-\omega(\xi p_\eta-\eta p_\xi)+\Theta, \tag{11}$$

where the ''force function'' is given by

$$\Theta=-\frac{1}{r}\mp F(\xi+x_0)+\frac{\omega_c^2}{8}(\xi^2+\eta^2)-\frac{1}{2}\omega^2x_0^2+\frac{1}{8}\omega_c^2x_0^2 + \left(\frac{\omega_c^2}{4}-\omega^2\right)x_0\xi, \tag{12}$$

and which may be expanded at x_0 [103] to produce an approximate Hamiltonian describing librations around L_m

$$\mathcal{H}=H+H_c,$$

where

$$H=\frac{p_\xi^2+p_\eta^2+p_\zeta^2}{2}+\frac{\omega^2}{2}(a\xi^2+b\eta^2+c\zeta^2)-\omega(\xi p_\eta-\eta p_\xi), \tag{13}$$

with

$$a=\frac{1}{\omega^2}\left(\frac{\omega_c^2}{4}-\frac{2}{x_0^3}\right), \quad b=\frac{1}{\omega^2}\left(\frac{\omega_c^2}{4}+\frac{1}{x_0^3}\right), \quad c=\frac{1}{\omega^2x_0^3}, \tag{14}$$

and H_c (the part of the Hamiltonian containing only constant terms) being given by

$$H_c=-\frac{1}{2}\omega^2x_0^2\mp Fx_0+\frac{1}{8}\omega_c^2x_0^2-\frac{1}{x_0}. \tag{15}$$

In the classical calculations H_c is ignored, although it provides a useful energy calibration in the quantum computations to be reported elsewhere [97]. The Hamiltonian H is identical in form to the cranked (anisotropic) oscillator that has been used in nuclear physics to generate basis vectors for self-consistent calculations to model collective rotations [104–107]. More recently, this problem has also been addressed (based on the Bogoliubov-Tyablikov transformation) in molecular physics to simplify rotational-vibrational Hamiltonians [108–111]. The motion in the ζ direction is stable and harmonic and, since it decouples from the planar motion in this approximation, need not be considered explicitly in the stability analysis that we are on the verge of performing.

B. Stability analysis of the equilibrium $L_m^{\max}$

As noted, a stability analysis [61,112] of this problem is only needed at the maximum, i.e., at the equilibrium $L_m^{\max}$. Restricting ourselves to first-order librations around $L_m^{\max}$ we define the vector

$$\Xi=(\xi,\eta,p_\xi,p_\eta) \tag{16}$$

and the matrix

$$\mathcal{A}=\begin{pmatrix} 0 & \omega & 1 & 0 \\ -\omega & 0 & 0 & 1 \\ -a\omega^2 & 0 & 0 & \omega \\ 0 & -b\omega^2 & -\omega & 0 \end{pmatrix}, \tag{17}$$

which allows Hamilton's equations to be written in the form

$$\dot{\Xi}=\mathcal{A}\Xi. \tag{18}$$

The stability of an equilibrium is determined by the eigenvalues of the matrix $\mathcal{A}$, i.e., the roots of the equation

$$\det(\lambda\mathcal{I}-\mathcal{A})=0, \tag{19}$$

where $\mathcal{I}$ is the unit matrix. Rather than solving this equation directly, we accept a suggestion of Deprit [113]: since $\det\mathcal{R}=1$ the matrix $\mathcal{R}$ can be inverted and we compute the matrix product $\mathcal{R}\mathcal{A}\mathcal{R}^{-1}$, where

$$\mathcal{R}=\begin{pmatrix} \lambda & -1 & 1 & 0 \\ 1 & \lambda & 0 & 1 \\ 1 & 0 & 0 & 0 \\ 0 & 1 & 0 & 0 \end{pmatrix}. \tag{20}$$

The eigenvalues are then determined as the roots of the polynomial equation

$$\det(\lambda\mathcal{I}-\mathcal{B})=0, \tag{21}$$

where

$$\mathcal{B}=\mathcal{R}\mathcal{A}\mathcal{R}^{-1}=\begin{pmatrix} \lambda & -1+\omega & 1-\lambda^2-a\omega^2 & \lambda-\lambda(-1+\omega)+\lambda\omega \\ 1-\omega & \lambda & -\lambda-\lambda(1-\omega)-\lambda\omega & 1-\lambda^2-b\omega^2 \\ 1 & 0 & -\lambda & 1+\omega \\ 0 & 1 & -1-\omega & -\lambda \end{pmatrix}. \tag{22}$$

The resulting polynomial equation

$$\det(\lambda\mathcal{I}-\mathcal{B})=\lambda^4+(2+a+b)\lambda^2\omega^2+(a-1)(b-1)\omega^4. \tag{23}$$

is considerably simpler to solve than Eq. (19). This is similar to the procedure for establishing linear stability (and the Routh critical value) in the RTBP. The motion is *linearly* stable if the four eigenvalues are purely imaginary; importantly, stable motion is possible even in the regime where the force function (i.e., the part of the Hamiltonian that depends solely on coordinates) corresponds to a saddle point—the rotation stabilizes the dynamics, in analogy to the situation in the Paul and Penning traps [75–78,82,83].

It is convenient to work with scaled frequencies and field strengths. In the original Hamiltonian (for the maximum) it is possible to scale the coordinates and momenta as follows: $\mathbf{r}'=\omega^{2/3}\mathbf{r}$, $\mathbf{p}'=\omega^{-1/3}\mathbf{p}$. After dropping the primes this yields for the Hamiltonian (2),

$$H=\mathcal{K}=\tfrac{1}{2}(p_x^2+p_y^2)-\frac{1}{r}-(xp_y-yp_x)+\tfrac{1}{8}\omega_s^2(x^2+y^2)+\epsilon x, \tag{24}$$

where $\mathcal{K}=K/\omega^{2/3}$, $\omega_s=\omega_c/\omega<2$ and $\epsilon=F/\omega^{4/3}$. This scaling shows that the *classical* dynamics depends only on the three parameters, $\mathcal{K}$, ω_s, and ϵ.

In the case $\omega_c=0$ the stable region for the problem in hand is extremely limited and results in a very restricted set of values that a and b may take for stable dynamics to be possible: specifically, the field parameters must be selected so that b lies in the range $\frac{8}{9}<b<1$ [49]. As one passes outside the stable regime a transition to instability [49] (Brown or Trojan bifurcation [61]) occurs at $L_m^{\max}$ when $\epsilon_c=F_c/\omega_f^{4/3}=\frac{1}{2}3^{-(4/3)}\approx 0.1156$, which limits the range of linear dynamics [49,48].

Figure 3 shows the regions of stable (shaded) and unstable (unshaded) motion at the maximum as a function of the parameters ω_s and ϵ. For $\omega_c\neq 0$ the curve separating stable from unstable motion consists of an upper branch ($\epsilon_c^{>}$) and a lower branch ($\epsilon_c^{<}$) given by [114]

$$\epsilon_c^{><}=\frac{4-5\omega_s^2\pm(2\pm\frac{1}{2}\omega_s^2)\sqrt{4-9\omega_s^2}}{2^{4/3}\omega_s^{2/3}(2\pm\sqrt{4-9\omega_s^2})^{2/3}}, \tag{25}$$

where the upper (lower) sign is taken throughout for $\epsilon_c^{>}$ ($\epsilon_c^{<}$). These two functions become equal to each other exactly at $\omega_s=\frac{2}{3}$, which is the rightmost point in Fig. 3. As one traverses the curve separating the stable from unstable regimes a Trojan bifurcation occurs—this is a generalization of the Trojan bifurcation for $\omega_c=0$ [49,48,61]. In general, as a function of ϵ and for fixed ω_s two transitions between stable and unstable motion occur, as, e.g., upon moving up the line $\omega_s=\frac{1}{2}$ in Fig. 3: first a transition to instability occurs at $\epsilon\approx\frac{1}{5}$ and then a transition back to stability at $\epsilon\approx\frac{3}{2}$. Interestingly, at the point labeled 5c in Fig. 3, where the two stability lines coincide, the problem becomes rigorously integrable, as can

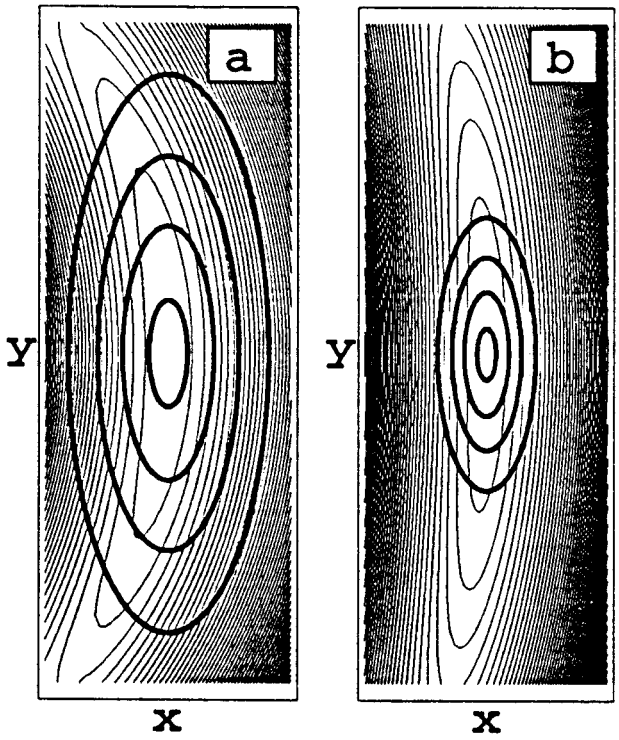

FIG. 7. Level curves of the ZVS at the maximum with $b=0.9562$—see Eq. (14). Thick lines are contours (at 0.25, 0.5, 0.75, and 0.95) of the Gaussian probability density centered at L_m (in a.u.); (a) $x_0=10^4$; (b) $x_0=10^7$. The axis scales in the x and y directions are equivalent, but, for clarity, the ranges of x and y are different.

be shown using results given by Raković and Chu [115–117]. At this point $\omega_c=\frac{2}{3}$ and $\epsilon_c=(2/3)^{4/3}$ and the Hamiltonian (19) reduces to

$$H=\tfrac{1}{2}(p_x^2+p_y^2)-\frac{1}{r}-(xp_y-yp_z)+\tfrac{1}{18}(x^2+y^2)+\epsilon_c x. \tag{26}$$

The classical motions that occur in the various regions of Fig. 3 will be explored shortly, but it is important to note that the stability diagram, Fig. 3, is obtained from a *linear* stability analysis that says nothing about the size of the stable region; it merely indicates for what parameter values some stable domain exists at $L_m^{\max}$. In particular, linear stability analysis contains no scale information and, therefore, if the stable volume of phase space is much smaller than $\hbar^3$, any putative coherent state will spread rapidly *despite* the stability of the maximum. This issue will be taken up again shortly. Our immediate task is to compute the local frequencies at the equilibria $L_m^{\max}$ and $L_m^{\min}$, and, thereby, compute the ground state of the cranked oscillator.

C. Coherent states

The four eigenvalues of $\mathcal{A}$ in the stable regime (either at the maximum or the minimum) are purely imaginary of the form $\pm i\Omega_\xi$ and $\pm i\Omega_\eta$, where $\Omega_{\xi,\eta}$ are positive, real numbers. After a rotation in phase space (described in detail in Refs. [104–107,109–111,108,97]),

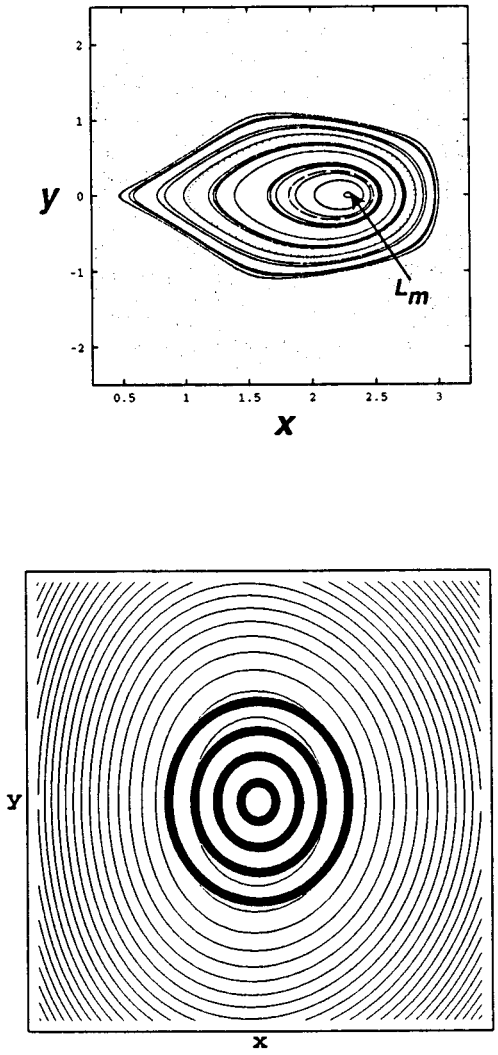

FIG. 8. Poincaré surfaces of section (a) around the maximum and (b) level curves of the ZVS for $\omega_f=1\times10^{-6}$, $\omega_c=5\times10^{-6}$, and $F=5\times10^{-8}$ a.u. In (b) the thick lines are contours (at 0.25, 0.5, 0.75, and 0.95) of the Gaussian probability density centered at $L_m=10^4$ a.u.

$$\begin{aligned}\xi' &= A\xi+Bp_\eta,\\ \eta' &= A\eta+Bp_\xi,\\ p'_\xi &= p_\xi+C\eta,\\ p'_\eta &= p_\eta+C\xi,\end{aligned} \tag{27}$$

with $A-BC=1$ (to preserve the commutation relations between coordinates and momenta), H can be reduced to the following separable form (here we follow the notation of Ref. [97] where a more complete treatment is provided):

$$H=\frac{1}{2m_\xi}p_\xi'^2+\tfrac{1}{2}m_\xi\Omega_\xi^2\xi'^2+\frac{1}{2m_\eta}p_\eta'^2+\tfrac{1}{2}m_\eta\Omega_\eta^2\eta'^2, \tag{28}$$

where

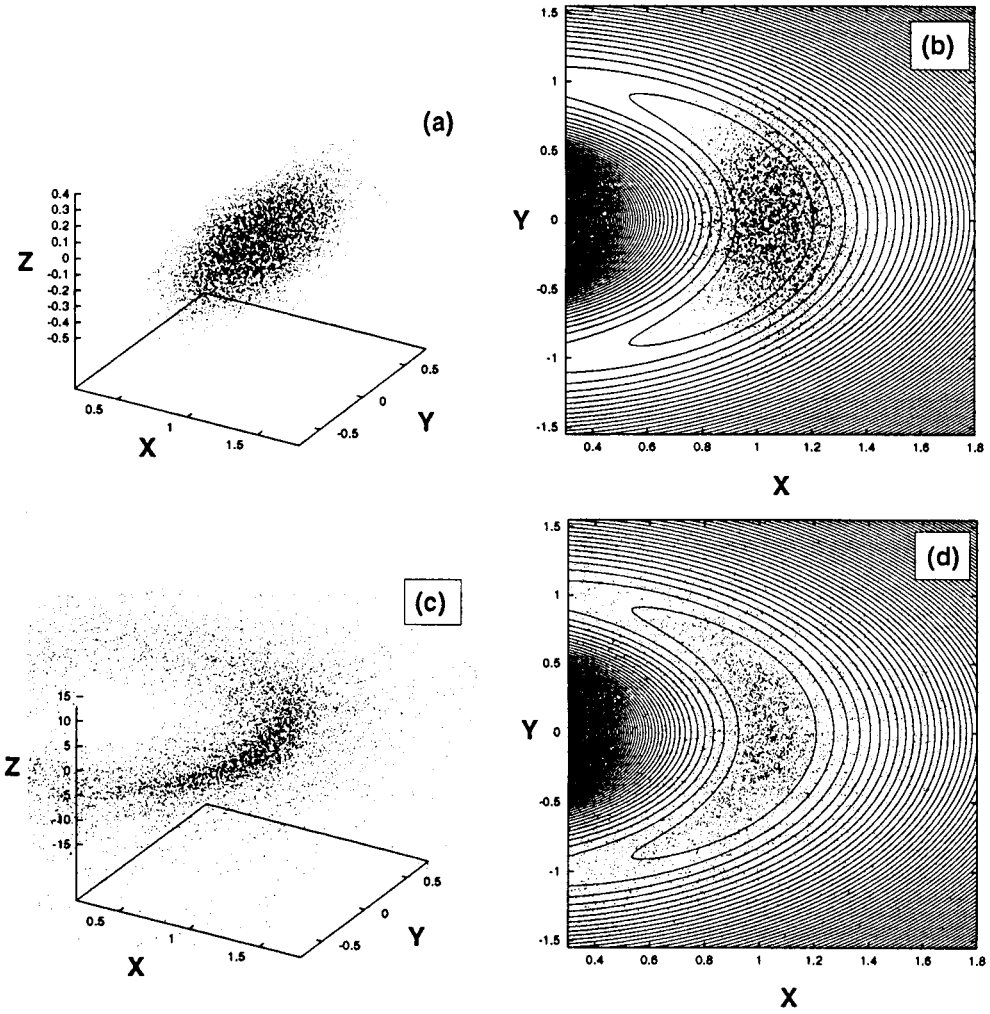

FIG. 9. Swarm of initial conditions plotted on the ZVS for the maximum with $\omega_c=0$ a.u., $\omega_f=4.629\,63\times10^{-6}$ a.u., $F=3.427\,47\times10^{-9}$ a.u., $K=-1.137\times10^{-3}$ a.u., and $x_0=3654.1$ a.u., at times after (a) and (b) 0, and (c) and (d) 796 Kepler orbits.

$$m_\xi=\frac{\Omega_\xi^2-\Omega_\eta^2}{\Omega_\xi^2-a\omega^2+\omega^2}$$

and

$$m_\eta=\frac{\Omega_\eta^2-\Omega_\xi^2}{\Omega_\eta^2-b\omega^2+\omega^2}, \tag{29}$$

with $\omega_\xi=|\omega|\sqrt{a}$, $\omega_\eta=|\omega|\sqrt{b}$, and $\omega_\zeta=|\omega|\sqrt{c}$. The eigenvalues are given by

$$E=\frac{m_\xi}{|m_\xi|}\,(n_\xi+\tfrac{1}{2})\hbar|\Omega_\xi|+\frac{m_\eta}{|m_\eta|}\,(n_\eta+\tfrac{1}{2})\hbar|\Omega_\eta|. \tag{30}$$

If the ground-state energy of the cranked oscillator is defined as $E_{00}=\hbar\Omega$, then the 3D vacuum state can be expressed as follows in terms of the original coordinates:

$$\Psi_{000}(x,y,z)=N\,\exp\left(-\frac{\alpha}{2}\,x^2-\frac{\beta}{2}\,y^2-\frac{\omega_\zeta}{2}\,z^2-i\,\gamma xy\right). \tag{31}$$

The parameters α,β,γ are given by

$$\alpha=\Omega(1+Q)/\hbar,$$

$$\beta=\Omega(1-Q)/\hbar,$$

$$\gamma=\omega Q/\hbar,$$

with

$$Q=\frac{(a-b)\omega^2}{4(\Omega^2-\omega^2)}, \tag{32}$$

and N is a normalization factor. In the simulations to follow, in this and in the companion paper [97], the procedure described above was used to generate a coherent state, either classically or quantum mechanically. The same general procedure is valid both at the maximum and at the minimum, although it is unnecessary at the minimum for the special case $\omega_f=\omega_c/2$, i.e., paramagnetic term eliminated. We also note that, quantum mechanically, the translation of coordinates to L_m introduces an additional phase factor into the wave packet (25) as described in [97]. This phase factor, like the term in γ in Eq. (31), has no *classical* consequences and is therefore ignored.

IV. CLASSICAL DYNAMICS AND GAUSSIAN SWARMS

In this section we study the classical dynamics of both the maximum and minimum configurations in light of the stability analysis presented in the preceding section. Included are simulations in which a swarm of classical particles is chosen

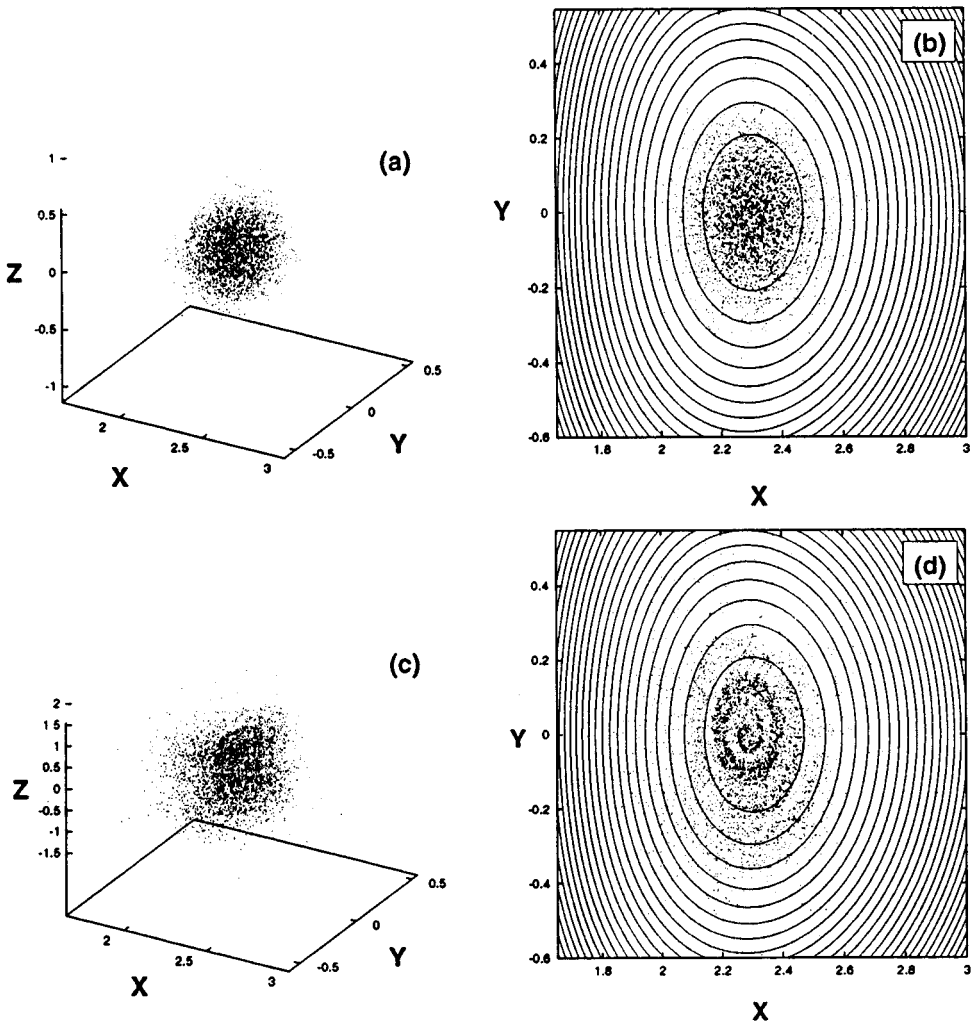

FIG. 10. Swarm of initial conditions plotted on the ZVS for the maximum with $\omega_c = 5\times10^{-6}$ a.u., $\omega_f = 1\times10^{-6}$ a.u., $F = 5\times10^{-8}$ a.u., $K = 10^{-4}$ a.u., and $x_0 = 10^4$ a.u., at times after (a) and (b) 0, and (c) and (d) 341 Kepler orbits.

with a spatial probability distribution given by $|\Psi(x,y,z)|^2$ and propagated in time classically to indicate how a quantum wave packet might behave. Of course, no phase information is included in the classical ''packet'' but such simulations are often found to be excellent predictors of the stability of quantum systems. In order to facilitate an understanding of the global dynamics and the possible existence of order-chaos transitions we also examine Poincaré surfaces of section in the planar limit. To avoid possible confusion the two configurations (maximum and minimum) are treated separately.

A. Dynamics at the maximum

While the classical simulations of quantum wave packets to be described later in this section are all 3D, for clarity, we first consider the 2D limit. We computed Poincaré surfaces of section (SOS) in the vicinity of $L_m^{\max}$ by integrating the equations of motion in cylindrical coordinates ($x=\rho\cos\phi$, $y=\rho\sin\phi$), computing the $P_\rho=0$ surface of section and plotting the x-y phase plane. (The classical scaling property means that all SOS are equivalent, independent of the value for x_0, at fixed ω_s and ϵ through mechanical similarity). In the absence of a magnetic field the regular regime surrounding $L_m^{\max}$ may be quite small—see Fig. 4—and the Kolmogorov-Arnold-Moser (KAM) islands are embedded in a sea of chaotic or scattering trajectories (ionization is possible because at energies greater than the saddle-point energy the electron can escape over the saddle [48].) As ϵ is increased further the KAM curves start to break up and the motion becomes increasingly chaotic, as illustrated in the sequence Figs. 4(a)–4(d), which shows the Trojan bifurcation that occurs at zero magnetic field.

The addition of a magnetic field ($\omega_c \neq 0$) changes the situation dramatically, since it is now possible to adjust the relative sizes of the coefficients a and b in order to enlarge the stable domain. In particular, it allows one to increase F beyond F_c, thereby increasing the size of the harmonic regime at $L_m^{\max}$. However, stable and unstable regimes still persist. Figures 5 and 6 show sequences of surfaces of section along the lines labeled AB and CD in Fig. 3 (the points in the parameter plane corresponding to the various surfaces of section in Figs. 5 and 6 are labeled on Fig. 3), and it is apparent that a sequence of order-chaos transitions occur. In Fig. 3 it is apparent that to the right of the line $\omega_s=\frac{2}{3}$, the motion is everywhere stable, although not necessarily integrable. At the point $\epsilon=(2/3)^{4/3}$, $\omega_s=\frac{2}{3}$ the two parts of the stability-instability curve coalesce and the corresponding surface of section is shown in Fig. 5(c). At this point the Hamiltonian is rigorously integrable, as can be shown using

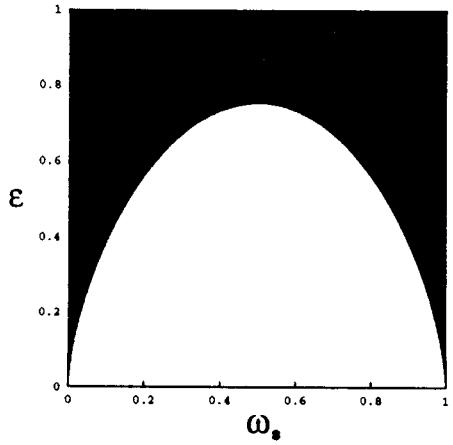

FIG. 11. Regions of parameter space for which the minimum exists (shaded): ω_s is the scaled frequency and ϵ is the scaled field strength as defined in the text.

results due to Raković and Chu [115–117] and as discussed above. The transition through the integrable limit is shown rather compellingly in the sequences 5(a)–5(d) and 6(a)–6(d). Interestingly, Figs. 6(a) and 6(b) show a ''shadow'' (a roughly hyperbolic blank area) that runs through the surface of section. We were unable to eliminate this feature despite integrating numerous trajectories in this region and choosing different surfaces of section. The shadows seem to be a result of the complicated topology of the torus that intersects the surface. Jaffé suggests using numerically determined orbits to define the surface of section and thereby to avoid such shadows [118]. Since the details of the surface of section in the vicinity of the maximum are unaffected we leave this point to a future study.

Figure 7(a) shows a Gaussian wave packet defined as in Ref. [49] and assuming $L_m^{\max}$ is located at $x_0=10^4$ a.u. (the value suggested in [49]) with $\epsilon=0.0444$ [49]. It is apparent that much of the packet spills out of the harmonic regime. If $x_0 \gtrsim 10^7$ a.u., however, most of the packet can fit quite comfortably into the harmonic part of the maximum—see Fig. 7(b). The stability of a Gaussian wave packet launched at $L_m^{\max}$ depends, in part, on the quality of a locally harmonic approximation to the ZVS at $L_m^{\max}$. If $F=0$ the ZVS is flat (i.e., not harmonic at all) transverse to the field direction in the rotating frame, but becomes increasingly harmonic with increasing F. However, for $\omega_c=0$, the Trojan bifurcation [61], which occurs at $L_m^{\max}$ when $\epsilon_c=F_c/\omega^{4/3}\approx 0.1156$, limits the range of linear dynamics. The magnetic field allows one to increase F beyond the critical value in the pure CP limit, thereby increasing the size of the harmonic regime at $L_m^{\max}$. Figure 8(a) shows the SOS for a typical set of magnetic and CP field strengths, and it is apparent that the size of the regular regime at L_m has been increased considerably as compared to the pure CP case. The corresponding coherent state is shown in Fig. 8(b). Figure 9 shows the time evolution of a 3D Gaussian swarm of initial conditions chosen to simulate the state shown in Fig. 7(a), and it is apparent that the swarm does not remain coherent but tends to spread along the curves of the ZVS. Contrast the case in Fig. 10, which is a simulation for the wave packet whose projection is shown in Fig. 8(b). In this case the swarm of initial conditions stays

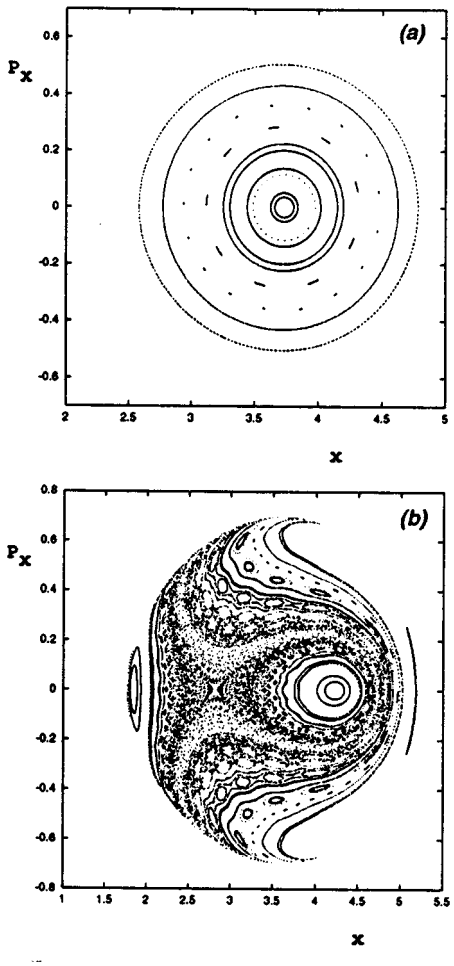

FIG. 12. Combined Poincaré surfaces of section for the minimum configuration with (a) $\epsilon=1$, $\Omega=\frac{1}{2}$, and $\mathcal{K}=-2.1$; (b) $\epsilon=0.9$, $\Omega=0.65$, and $\mathcal{K}=-1.85$.

roughly coherent. All calculations are in scaled units.

B. Dynamics at the minimum

Before examining the dynamics in detail it is illuminating, first, to consider two particular limits of the ZVS,

$$V=-\frac{1}{r}+\frac{\omega_f(\omega_c-\omega_f)}{2}(x^2+y^2)-Fx. \tag{33}$$

(a) in the $E\times B$ limit ($\omega_f=0$) the effective potential is

$$V=-\frac{1}{r}+Fx. \tag{34}$$

Clearly, the ionization threshold is given by the simple Stark saddle-point (SSP) criterion [84,86,87], despite the presence of the magnetic field. Classically, ionization is possible (but not inevitable) whenever the energy exceeds the energy of the saddle point. Note that, while a double well may exist in the ''potential,'' defined artificially by setting the generalized momenta $p_x=p_y=0$ in Eq. (2) [92–94], no such struc-

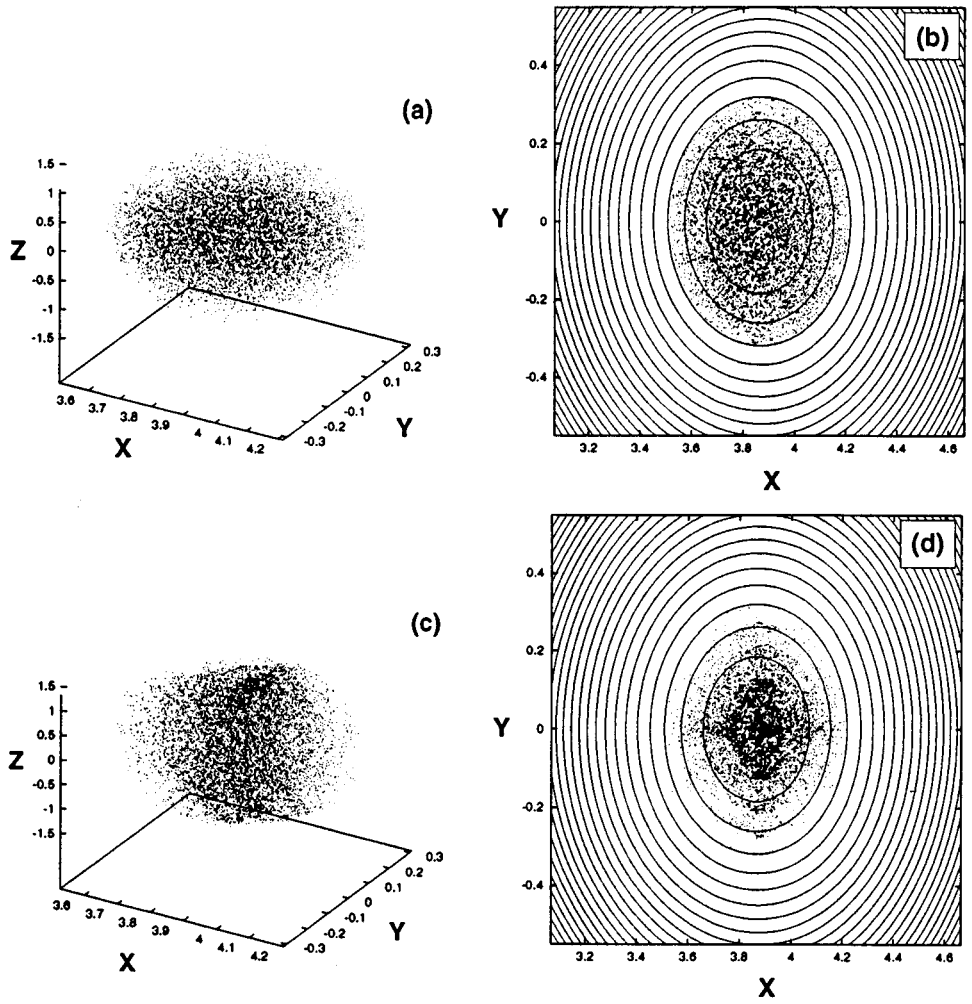

FIG. 13. Swarm of initial conditions plotted on the ZVS for the minimum trap with $\omega_c = 1.519\,83\times10^{-5}$ a.u., $\omega_f = 7.599\,15\times10^{-7}$ a.u., $F = 3.889\,43\times10^{-7}$ a.u., $\epsilon = 1.033\,14$ a.u., $K = -1.454\,62\times10^{-2}$ a.u., and $x_0 = 6298.79$ a.u., at times after (a) and (b) 0, and (c) and (d) 597 Kepler orbits.

ture can occur in the ZVS—essentially, ionization is only possible because of the presence of the paramagnetic term in the static crossed-fields system.

(b) The pure CP (i.e., $\omega_c = 0$) problem is more complicated: the effective potential is given by

$$V = -\frac{1}{r} - \frac{\omega_f^2}{2}(x^2+y^2) + Fx, \tag{35}$$

and the electron may escape if its energy lies above the saddle point in the ZVS, although above threshold, bound, classical motion is also possible [48]. However, the ionization mechanism in the CP case is considerably more intricate than for the $E\times B$ problem, involving destabilization through a Trojan bifurcation [48,61].

The system under study differs considerably from these two limits in that the coefficient of the term in (x^2+y^2) in

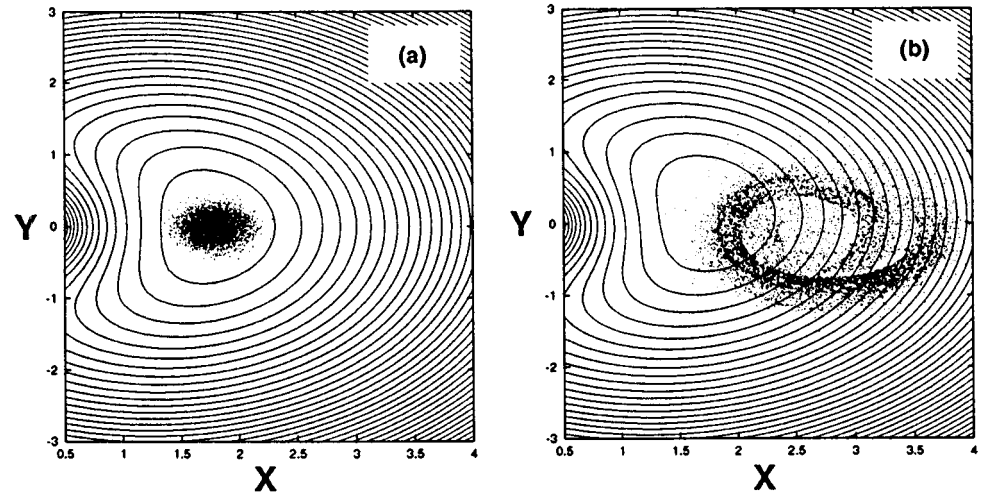

FIG. 14. Swarm of initial conditions with an elliptically polarized field; ω_c, ω_f, and F are the same as for Fig. 10, $\alpha_1 = 0.6$ and $\alpha_2 = 1.0$. Initial Gaussian (a) at $t = 0$; (b) after 500 Kepler orbits.

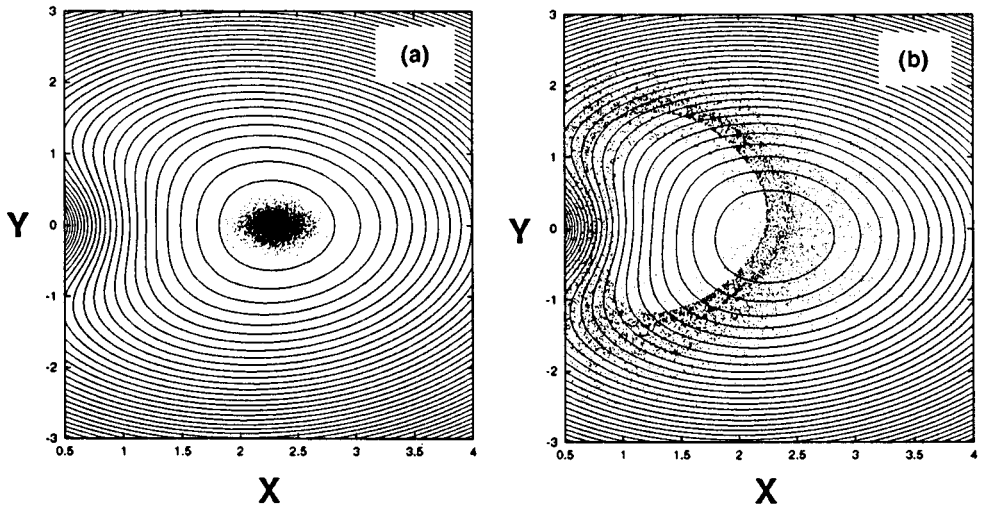

FIG. 15. Swarm of initial conditions with an elliptically polarized field; ω_c, ω_f, and F are the same as for Fig. 10, $\alpha_1=1.0$ and $\alpha_2=0.6$. Initial Gaussian (a) at $t=0$; (b) after 500 Kepler orbits.

the ZVS can be arranged to be nonzero and positive, thus confining the electron (in the planar limit) irrespective of the size of F. This occurs whenever $\omega_c-\omega_f>0$, provided that $\omega_f\neq 0$. For a given ω_c this coefficient is maximized when $\omega_f=\omega_c/2$, i.e., the paramagnetic term in Eq. (2) is absent, and the ZVS becomes equivalent to a true potential-energy surface (this case is illustrated in Fig. 2). In the 3D Hamiltonian, however, ionization is possible but only along the z direction. The ionization energy threshold is given by

$$E_{\rm ion}=-\frac{F^2}{2\omega_f(\omega_c-\omega_f)} \tag{36}$$

and all of the 3D simulations we report fall below this value.

Again, it is convenient to scale coordinates and momenta, although in a different way than previously since now the coefficient of the paramagnetic term ω can be zero: explicitly the scaling is $\mathbf{r}'=\omega_c^{2/3}\mathbf{r}$, $\mathbf{p}'=\omega_c^{-1/3}\mathbf{p}$. After dropping the primes this yields the Hamiltonian

$$H=\mathcal{K}=\tfrac{1}{2}(p_x^2+p_y^2+p_z^2)-\frac{1}{r}-(\Omega-\tfrac{1}{2})(xp_y-yp_x)$$
$$+\tfrac{1}{8}(x^2+y^2)+\epsilon x. \tag{37}$$

where $\mathcal{K}=K/\omega_c^{2/3}$, $\Omega=\omega_f/\omega_c$, and $\epsilon=F/\omega_c^{4/3}$. This scaling shows that the dynamics depends only on the three parameters, $\mathcal{K}$, Ω, and ϵ. Figure 11 shows the region of parameter space for which the minimum exists.

Figure 12(a) is a typical Poincaré surface of section of the planar ($z=0$) Hamiltonian for a value of $\mathcal{K}$ midway between the minimum and the saddle point. The figure clearly shows stable motion localized in the well in the ZVS. Interestingly, for the special value of $\Omega=\frac{1}{2}$, (i.e., paramagnetic term absent) in Fig. 12(a) the dynamics in the well is essentially harmonic and, in fact, the planar system is actually integrable in this limit. The possible integrability of this Hamiltonian was evidently first speculated on in Ref. [91]; in fact, the Hamiltonian is of Stäckel form and separates in elliptical coordinates [119–122]. For values of $\Omega\neq\frac{1}{2}$ it is possible for the motion to be chaotic within the well, as shown in Fig. 12(b). Provided that tunneling is unimportant the electron will still be confined in the well by the curves of zero velocity for all values of K below both the saddle point and $E_{\rm ion}$. A typical 3D swarm of initial conditions is shown in Fig. 13 and it is apparent that the swarm stays extremely compact and localized at the minimum in the ZVS.

C. Elliptical polarization and pulsating zero velocity surfaces

It is apparent that in an actual experiment it might not be feasible to prepare microwave radiation whose polarization is exactly circular. In this subsection we examine the effect of relatively small deviations from circularity for Gaussian swarms started at the maximum. Results for the minimum are similar, and, in general, the minimum is even more robust than the maximum to such deviations. We consider only the planar limit ($z=0$) for which the Hamiltonian for a hydrogen atom in an elliptically polarized microwave field and an orthogonal magnetic field is

$$H=\frac{p_x^2+p_y^2}{2}-\frac{1}{r}-\frac{1}{2}\,\omega_c(xp_y-yp_x)+\frac{\omega_c^2}{8}\,(x^2+y^2)$$
$$+F(\alpha_1 x\,\cos\omega_f t+\alpha_2 y\,\sin\omega_f t), \tag{38}$$

where α_1 and α_2 are parameters that control the ellipticity of the field; e.g., circular polarization is given by $\alpha_1=\alpha_2$. We move to a frame rotating with the microwave frequency, which results in an explicitly time-dependent Hamiltonian where the driving terms result from the ellipticity of the field. It is possible, proceeding as before, to construct a ZVS that is now time dependent, i.e., the surface pulsates in time. Figures 14 and 15 show the long-term behavior of a Gaussian swarm after 500 Kepler periods for (i) $\alpha_1=0.6$, $\alpha_2=1.0$ and (ii) $\alpha_1=1$, $\alpha_2=0.6$, respectively. In both cases the swarm was started at the equilibrium point assuming exactly CP radiation, and it is apparent that, while the swarm does not stay Gaussian, neither does it dissipate. For less severe, but still quite strong, deviations from pure CP radiation the packet tends to stay together, as illustrated in Fig. 16, which shows (a) the initial Gaussian, and (b)–(g) the time evolution of the packet on the pulsating ZVS during the last Kepler cycle of the integration. These results suggest that even fairly substantial deviations from ellipticity are not sufficient to de-

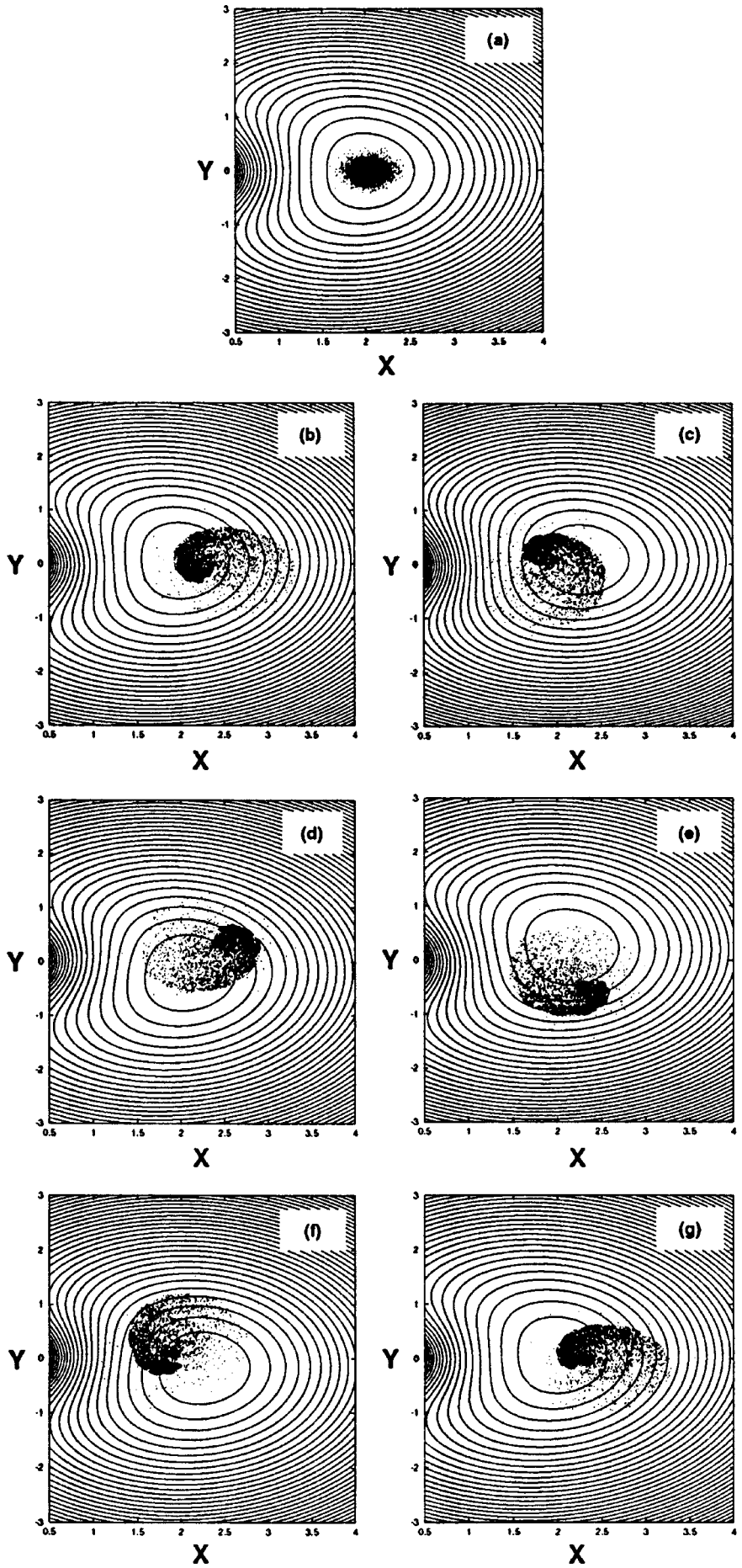

FIG. 16. Swarm of initial conditions with an elliptically polarized field; ω_c, ω_f, and F are the same as for Fig. 10, $\alpha_1=0.8$ and $\alpha_2=1.0$. Initial swarm (a) at $t=0$; (b) after 499.0, (c) after 499.2, (d) after 499.4, (e) after 499.6, (f) after 499.8, and (g) after 500.0 rev.

stroy the coherence of the packet. We note that the concept of pulsating coordinates and a pulsating ZVS has been used in celestial mechanics in the elliptical restricted three-body problem, as described by Murison [123].

V. CONCLUSIONS

We have investigated the dynamics of a hydrogen atom subjected simultaneously to a circularly polarized microwave field and a magnetic field perpendicular to the plane of polarization. Stability analysis and classical simulations reveal that the magnetic field can be used to stabilize wave packets prepared at the global equilibrium point against dispersion and spreading. In the harmonic approximation these states are identical to the coherent states of the cranked harmonic oscillator and behave accordingly, as coherent states. The essential classical predictions are found, in the companion paper [97], to be borne out in numerically accurate quantum FFT computations. Finally we note that the results in this paper may have applications to excitonic systems in crossed (static) electric and magnetic fields where the coefficient of the paramagnetic term may vary as the effective masses of the hole and electron vary [91,124–126] and also in the positronium atom where this term vanishes [127].

ACKNOWLEDGMENTS

We thank Professor T. Uzer, Dr. Charles Cerjan, and Professor Charles Jaffé for helpful suggestions. Support of this work by the American Chemical Society (Petroleum Research Fund) is gratefully acknowledged.

[1] E. Rutherford, Philos. Mag. **21**, 669 (1911).
[2] E. Nagaoka, Philos. Mag. **7**, 445 (1904).
[3] M. Born, *The Mechanics of the Atom*, 2nd ed., translated by J. W. Fisher (Ungar, New York, 1960), pp. 130–241.
[4] M. Nauenberg, C. Stroud, and J. A. Yeazell, Sci. Am. **270**, 44 (1994).
[5] G. Raithel, M. Fauth, and H. Walther, Phys. Rev. A **47**, 419 (1991).
[6] J. A. Yeazell and C. R. Stroud, Phys. Rev. A **43**, 5153 (1991).
[7] T. F. Gallagher, *Rydberg Atoms* (Cambridge University Press, Cambridge, 1994).
[8] L. S. Brown, Am. J. Phys. **41**, 525 (1973).
[9] D. R. Snieder, Am. J. Phys. **51**, 801 (1983).
[10] J. Mostowski, Lett. Math. Phys. **2**, 1 (1977).
[11] C. C. Gerry, Phys. Rev. A **33**, 6 (1986); B. R. Johnson, *ibid.* **35**, 1412 (1987).
[12] D. Bhaumik, B. Dutta-Roy, and G. Gosh, J. Phys. A **19**, 1353 (1986).
[13] S. Nandy and C. S. Shastry, J. Phys. A **22**, 1005 (1989).
[14] M. Nauenberg, Phys. Rev. A **40**, 1133 (1989).
[15] J. C. Gay, D. Delande, and A. Bommier, Phys. Rev. A **39**, 6587 (1989).
[16] D. S. McAnnally, and A. J. Bracken, J. Phys. A **23**, 2027 (1990).
[17] Z. D. Gaeta and C. R. Stroud, Phys. Rev. A **42**, 6308 (1990).
[18] C. Lena, D. Delande, and J. C. Gay, Europhys. Lett. **15**, 697 (1991).
[19] J. R. Klauder, J. Phys. A **29**, L293 (1996).
[20] G. Alber and P. Zoller, Phys. Rep. **199**, 231 (1991).
[21] L. Marmet, H. Held, G. Raithel, J. A. Yeazell, and H. Walther, Phys. Rev. Lett. **72**, 3779 (1994).
[22] J. Wals *et al.*, Phys. Rev. Lett. **72**, 3783 (1994).
[23] W. M. Zhang, D. H. Feng, and R. Gilmore, Rev. Mod. Phys. **62**, 867 (1990).
[24] E. Schrödinger, Naturwissenschaften **14**, 664 (1926).
[25] E. Schrödinger, in *Letters in Wave Mechanics*, edited by K. Prizibram (Philosophical Library, New York, 1967).
[26] P. Kustaanheimo and E. Stiefel, J. Reine Angew. Math. **218**, 204 (1965).
[27] A. Deprit, A. Elipe, and S. Ferrer, Celest. Mech. and Dynam. Astron., **58**, 151 (1994).
[28] A. O. Barut and B. W. Xu, Helv. Phys. Acta. **66**, 712 (1993).
[29] J. A. Yeazell and C. R. Stroud, Phys. Rev. Lett. **60**, 1494 (1988).
[30] R. J. Brecha, G. Raithel, C. Wagner, and H. Walther, Opt. Commun. **102**, 257 (1993).
[31] P. Nussenzveig, F. Bernardot, M. Brune, J. Hare, J. M. Raimond, S. Haroche, and W. Gavlik, Phys. Rev. A **48**, 3991 (1993).
[32] M. Mallalieu and C. R. Stroud, Phys. Rev. A **49**, 2329 (1994).
[33] M. Mallalieu and C. R. Stroud, Phys. Rev. A **51**, 1827 (1995).
[34] Z. D. Gaeta, M. W. Noel, and C. R. Stroud, Phys. Rev. Lett. **73**, 636 (1994).
[35] J. A. Yeazell, M. Mallalieu, and C. R. Stroud, Phys. Rev. Lett. **61**, 1938 (1988).
[36] J. A. Yeazell, M. Mallalieu, and C. R. Stroud, Phys. Rev. A **40**, 5040 (1989).
[37] C. Raman, C. W. S. Conover, C. I. Sukenik, and P. H. Bucksbaum, Phys. Rev. Lett. **76**, 2436 (1996).
[38] D. W. Schumaker, J. H. Hoogenraad, D. Pinkos, and P. H. Bucksbaum, Phys. Rev. A **52**, 4719 (1996).
[39] M. W. Noel and C. R. Stroud, Phys. Rev. Lett. **75**, 1252 (1995).
[40] R. G. Hulet and D. Kleppner, Phys. Rev. Lett. **51**, 1430 (1983).
[41] W. A. Molander, C. R. Stroud, and J. A. Yeazell, J. Phys. B **19**, L461 (1986).
[42] C. H. Cheng, C. Y. Lee, and T. F. Gallagher, Phys. Rev. Lett. **73**, 3078 (1994).
[43] J. Hare, M. Gross, and P. Goy, Phys. Rev. Lett. **73**, 3078 (1994).
[44] S. B. Hansen *et al.*, Phys. Rev. Lett. **71**, 1522 (1993).
[45] K. S. Mogensen *et al.*, Phys. Rev. A **51**, 4038 (1995).
[46] A. Bommier, D. Delande, and J. C. Gay, *Atoms in Strong Fields*, edited by C. A. Nicolaides *et al.* (Plenum, New York, 1990).
[47] R. J. Glauber, Phys. Rev. **130**, 2529 (1963).
[48] D. Farrelly and T. Uzer, Phys. Rev. Lett. **74**, 1720 (1995).

[49] I. Bialynicki-Birula, M. Kaliński, and J. H. Eberly, Phys. Rev. Lett. **73**, 1777 (1994).
[50] P. Fu, T. J. Scholz, J. M. Hettema, and T. F. Gallagher, Phys. Rev. Lett. **64**, 511 (1990).
[51] C. H. Cheng, C. Y. Lee, and T. F. Gallagher, Phys. Rev. Lett. **73**, 3078 (1994).
[52] M. Nauenberg, Phys. Rev. Lett. **64**, 2731 (1990).
[53] M. Nauenberg, Europhys. Lett. **13**, 611 (1990).
[54] P. Kappertz and M. Nauenberg, Phys. Rev. A **47**, 4749 (1993).
[55] J. A. Griffiths and D. Farrelly, Phys. Rev. A **45**, R2678 (1992).
[56] K. Rzazewski and B. Piraux, Phys. Rev. A **47**, R1612 (1993).
[57] A. Peregrine-Smew, D. Farrelly, and T. Uzer, Phys. Rev. A **51**, 4293 (1995).
[58] D. Farrelly, P. Bellomo, and T. Uzer, Phys. Rev. Lett. **74**, 3495 (1995).
[59] G. W. Hill, Am. J. Math. **1**, 5 (1878).
[60] V. Szebehely, *Theory of Orbits: The Restricted Problem of Three Bodies* (Academic, New York, 1967).
[61] R. Abraham and J. E. Marsden, *Foundations of Mechanics*, 2nd ed. (Addison-Wesley, Redwood City, CA, 1987), pp. 675–688.
[62] D. Farrelly, E. Lee, and T. Uzer, Phys. Rev. Lett. **75**, 972 (1995).
[63] I. Bialynicki-Birula, M. Kaliński, and J. H. Eberly, Phys. Rev. Lett. **75**, 973 (1995).
[64] J. Zakrzewski, R. Gebarowski, and D. Delande, Phys. Rev. A **54**, 691 (1996).
[65] M. Kaliński, J. H. Eberly, and Bialynicki-Birula, Phys. Rev. A **52**, 2460 (1995).
[66] M. Kaliński and J. H. Eberly, Phys. Rev. A **53**, 1715 (1996).
[67] M. Kaliński, J. H. Eberly, and Bialynicki-Birula, Phys. Rev. A **52**, 4285 (1995).
[68] D. Delande, J. Zakrzewski, and A. Buchleitner, Europhys. Lett. **32**, 107 (1995).
[69] J. Zakrzewski, D. Delande, and A. Buchleitner, Phys. Rev. Lett. **75**, 4015 (1995).
[70] A. Buchleitner, B. Grémand, and D. Delande, J. Phys. B **55**, 1622 (1985).
[71] A. Maquet, S. I. Chu, and W. P. Reinhardt, Phys. Rev. A **27**, 2946 (1983).
[72] D. Farrelly, E. Lee, and T. Uzer, Phys. Lett. A **204**, 359 (1995).
[73] E. Lee, A. F. Brunello, and D. Farrelly, Phys. Rev. Lett. **75**, 3641 (1994).
[74] A. F. Brunello, T. Uzer, and D. Farrelly, Phys. Rev. Lett. **76**, 2874 (1996). The contour plots of eigenstates shown in this Letter and also those for the Trojan states in [68] (i.e., at the maximum) seem to adopt the shape of the level curves of the underlying ZVS.
[75] W. Paul, Rev. Mod. Phys. **62**, 531 (1992).
[76] F. M. Penning, Rev. Mod. Phys. **3**, 873 (1936).
[77] H. Dehmelt, Rev. Mod. Phys. **62**, 525 (1992).
[78] L. S. Brown and G. Gabrielese, Rev. Mod. Phys. **58**, 2335 (1986).
[79] J. Schmiedmayer, Z. Phys. D **60**, 169 (1995).
[80] J. E. Bayfield, G. Casati, I. Guarneri, and D. W. Sokol, Phys. Rev. Lett. **63**, 364 (1989).
[81] R. Blümel, J. M. Chen, E. Peik, W. Quint, W. Schleich, and H. Walther, **334**, 309 (1988).
[82] D. Farrelly and J. E. Howard, Phys. Rev. A **48**, 851 (1993); **49**, 1494 (1994).
[83] J. E. Howard and D. Farrelly, Phys. Lett. A **178**, 62 (1993).
[84] C. W. Clark, E. Korevaar, and M. G. Littman, Phys. Rev. Lett. **54**, 320 (1985).
[85] C. Nessman and W. P. Reinhardt, Phys. Rev. A **35**, 3269 (1987).
[86] G. Raithel, M. Fauth, and H. Walther, Phys. Rev. A **44**, 1898 (1991).
[87] G. Wiebusch, J. Main, K. Kruger, H. Rottke, A. Holle, and K. H. Welge, Phys. Rev. Lett. **62**, 2821 (1989).
[88] G. Raithel and H. Walther, Phys. Rev. A **49**, 1646 (1993).
[89] J. Main and G. Wunner, Phys. Rev. Lett. **44**, 1898 (1992).
[90] M. J. Gourlay, T. Uzer, and D. Farrelly, Phys. Rev. A **47**, 3113 (1993).
[91] D. Farrelly, Phys. Lett. A **191**, 265 (1994).
[92] J. C. Gay, L. R. Pendrill, and B. Cagnac, Phys. Lett. A **72**, 315 (1979).
[93] L. A. Burkova, I. E. Dzyaloshinskii, G. F. Drukarev, and B. S. Monozon, Zh. Eksp. Teor. Fiz. **71**, 526 (1976) [Sov. Phys. JETP **44**, 276 (1976)].
[94] S. K. Bhattacharya and A. R. P. Rau, Phys. Rev. A **26**, 2315 (1982).
[95] L. I. Gorkov and I. E. Dzyaloshinski, Zh. Eksp. Teor. Fiz. **53**, 717 (1967) [Sov. Phys. JETP **26**, 449 (1968)].
[96] O. Dippel, P. Schmelcher, and L. S. Cederbaum, Phys. Rev. A **49**, 4415 (1994).
[97] C. Cerjan, E. Lee, D. Farrelly, and T. Uzer, **55**, 2222 (1997).
[98] A. Deprit, in *The Big Bang and George Lemaitre*, edited by A. Berger (Reidel, Dordrecht, 1984), pp. 151–180.
[99] K. Weierstrass, in *Weierstrass: Mathematische Werke*, reprinted (Olms and Johnson, Hildesheim, 1967), Vol. 1, pp. 233–246; R. S. MacKay, in *Nonlinear Phenomena and Chaos*, edited by S. Sarkar (Hilger, Bristol, 1986), pp. 254–270.
[100] R. Greenberg and D. R. Davis, Am. J. Phys. **46**, 1068 (1978).
[101] A. Deprit, Astron. J. **71**, 77 (1966).
[102] A. Deprit and A. Deprit-Bartholomé, Astron. J. **72**, 173 (1966).
[103] A. Deprit and A. Delie, Icarus **4**, 242 (1965).
[104] A. Bohr and B. R. Mottelson, *Nuclear Structure* (Benjamin, Reading, MA, 1975), Vol. II, pp. 84–88.
[105] K. F. Liu and G. Ripka, Nucl. Phys. A **293**, 333 (1977).
[106] D. Glas, U. Mosel, and P. G. Zint, Z. Phys. **285**, 83 (1978).
[107] M. A. Z. Habeeb, J. Phys. G **13**, 651 (1987).
[108] D. Farrelly, T. Uzer, P. E. Raines, J. P. Skelton, and J. A. Milligan, Phys. Rev. A **45**, 4738 (1992).
[109] N. N. Bogoliubov, *Lectures on Quantum Systems, Vol. I, Quantum Statistics* (Gordon and Breach, New York, 1967).
[110] S. V. Tyablikov, *Methods in the Quantum Theory of Magnetism* (Plenum, New York, 1967).
[111] M. S. Krishnan and T. Carrington, Jr., J. Chem. Phys. **94**, 461 (1991).
[112] J. E. Howard and R. S. MacKay, J. Math. Phys. (N.Y.) **28**, 1036 (1987).
[113] A. Deprit (private communication).
[114] V. Lanchares, M. Iñarrea, J. P. Salas, E. Lee, and D. Farrelly (unpublished).
[115] M. J. Raković and S. I. Chu, Phys. Rev. A **50**, R5077 (1994).
[116] M. J. Raković and S. I. Chu, Physica D **81**, 271 (1995).
[117] M. J. Raković and S. I. Chu, Phys. Rev. A **52**, 1358 (1995).

[118] C. Jaffé (private communication). Imagine a torus that is folded such that a slice through it looks like a double well. When the two ''minima'' touch the surface of section, that surface will show features that look like periodic orbits (i.e., two points) that grow into two islands as in Figs. 6(a) and 6(b). This may happen even though no true *resonance* islands are actually present. Further tucks and creases in the torus can produce parts that never intersect the section giving the appearance of shadows in the numerical plots. Shadows are a telltale sign of this phenomenon.

[119] D. Apostolakis, E. G. Floratos, and N. D. Vlachos (unpublished).

[120] M. J. Raković, T. Uzer, and D. Farrelly (unpublished).

[121] In Ref. [73] we speculated that, while the problem might be integrable, it likely was not separable based on comparison with harmonic generation results in a similar Hamiltonian by Zuo *et al.* [122]. In fact, the Hamiltonian separates in displaced elliptical coordinates [119].

[122] T. Zuo, A. D. Bandrauk, M. Ivanov, and P. B. Corkum, Phys. Rev. A **51**, 3991 (1995).

[123] M. Murison, Ph.D. thesis, University of Wisconsin, 1988 (unpublished).

[124] I. Dzyaloshinskii, Phys. Lett. A **165**, 69 (1992).

[125] D. Baye, N. Clerbaux, and M. Vincke, Phys. Lett. A **166**, 135 (1992).

[126] B. R. Johnson, J. O. Hirschfelder, and K. H. Yang, Rev. Mod. Phys. **55**, 109 (1988).

[127] P. Schmelcher, J. Phys. B **25**, 2697 (1992).